Beyond Rewards: a Hierarchical Perspective on Offline Multiagent Behavioral Analysis

Anonymous Author(s)
Affiliation
Address
email

Abstract

Each year, expert-level performance is attained in increasingly-complex multiagent domains, notable examples including Go, Poker, and StarCraft II. This rapid progression is accompanied by a commensurate need to better understand how such agents attain this performance, to enable their safe deployment, identify limitations, and reveal potential means of improving them. In this paper we take a step back from performance-focused multiagent learning, and instead turn our attention towards agent behavior analysis. We introduce a model-agnostic method for discovery of behavior clusters in multiagent domains, using variational inference to learn a hierarchy of behaviors at the joint and local agent levels. Our framework makes no assumption about agents' underlying learning algorithms, does not require access to their latent states or policies, and is trained using only offline observational data. We illustrate the effectiveness of our method for enabling the coupled understanding of behaviors at the joint and local agent level, detection of behavior changepoints throughout training, discovery of core behavioral concepts, demonstrate the approach's scalability to a high-dimensional multiagent MuJoCo control domain, and also illustrate that the approach can disentangle previously-trained policies in OpenAI's hide-and-seek domain.

1 Introduction

Multiagent approaches have driven numerous advances in artificial intelligence research, with seminal examples including TD-gammon [1], DeepBlue [2], AlphaGo [3], AlphaZero [4], Libratus [5], AlphaStar [6], OpenAI Five [7], and Pluribus [8]. During training, many of these approaches seek to push the performance of agents as measured by a reward signal, or derivatives thereof.

Despite this, post-hoc methods that seek to *understand* agent interactions often use less reward-centric techniques. Instead, insights are drawn from behavioral analysis to identify unique or interesting agent strategies. Examples include clustering-based analysis of neuron activations and trajectories in capture-the-flag [9], inspection of trajectories in a hide-and-seek domain to detect interesting behaviors such as agents that learn to exploit the underlying physics engine [10], monitoring of statistics such as pass ranges and frequencies in humanoid football [11], and analysis of AlphaZero's acquisition of chess knowledge [12]. Crucially, such insights are often drawn via manual analysis and detection of behavioral clusters, or use of statistics associated with certain behaviors as defined by humans experts (e.g., various skills and relevant metrics in humanoid football).

As evident above, understanding emergent multiagent behaviors is enriched by techniques beyond pure reward-based analysis, as behavioral signifiers are not always discernible via rewards. Figure 1a provides intuition on this notion, illustrating returns (sum of rewards) throughout training for a multiagent hill-climbing domain (later described in detail). We highlight two independent training trials (A and B) with similar final returns. Despite this, comparing the trajectories generated via the

Submitted to 36th Conference on Neural Information Processing Systems (NeurIPS 2022). Do not distribute.

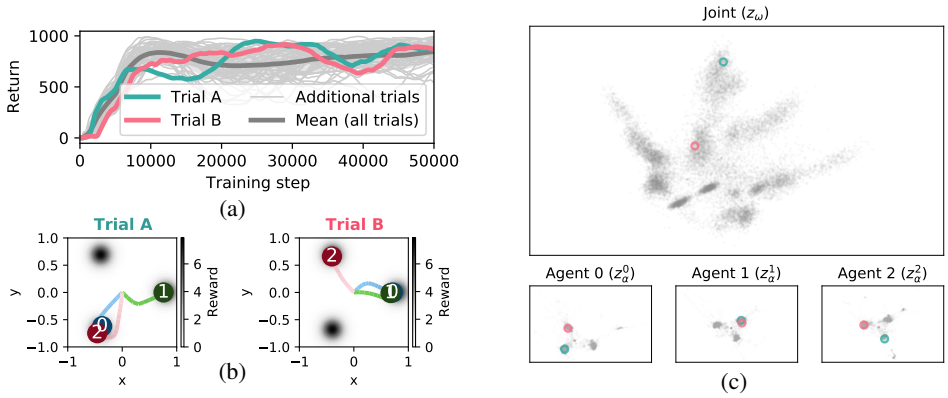

Figure 1: Reward alone is not enough to understand underlying behaviors in a 3-agent hill-climbing domain. Agents here start at the origin, each receiving rewards by navigating to any of 3 equidistant hills. (a) visualizes the total returns of agents throughout training, over 50 independent trials. Two trials (A and B) with similar final returns are highlighted. (b) visualizes the actual converged behaviors of the agents at the end of Trials A and B, which are distinct despite their similar returns. Visualizing these same trajectories in the behavior space learned by our approach immediately reveals differences in the joint behavior of agents in the top panel of (c), where the two color markers correspond to the trajectories from each trial. Simultaneously analyzing the agent-wise latent spaces in the bottom 3 panels of (c) highlight that agent 1 behaves the same way in both trials, in contrast to agents 0 and 2.

agents' deterministic policies at the end of each trial's training (Fig. 1b) reveals entirely different behaviors. Analogous examples are evident in the above works (e.g., Fig. 1 of Baker et al. [10], where substantial behavior changes occur in multiagent hide-and-seek despite a smooth reward curve).

This paper formalizes the problem of offline multiagent behavior analysis. Our proposed algorithm, Multiagent Offline Hierarchical Behavior Analyzer (MOHBA), learns a hierarchical latent space that simultaneously reveals behavior clusters at the joint level (i.e., interactions *between* agents) and local level (i.e., behaviors of *individual* agents). Our method is agnostic of the underlying algorithm used to generate agents' behaviors, requires no access or control of the underlying environment, does not assume availability of a reward signal, and does not require access to agents' models or internal states. Our experiments investigate the structure of the learned behavior space, which goes beyond prior works on latent-clustering by identifying relationships between individual agent and joint behaviors. We illustrate that clusters identified by MOHBA are useful for highlighting similarities and differences in behaviors throughout training. We also quantitatively analyze the completeness of discovered behavior clusters by adopting a modified version of the concept-discovery framework of Yeh et al. [13] to identify interesting behavior concepts in our multiagent setting. We then test the scalability of our approach by using it for behavioral analysis of several high-dimensional multiagent MuJoCo environments [14]. Finally, we evaluate the approach on the open-sourced OpenAI hide-and-seek policy checkpoints [10], confirming that the behavioral clusters detected by MOHBA closely match those of the human-expert annotated labels provided in their policy checkpoints.

2 Related Work

Significant research has been conducted in single-agent skill discovery, which seeks to learn reusable policies useful for downstream tasks [15–28]. Related approaches discover motor primitives to express longer-horizon policies [29], including use of offline reinforcement learning (RL) for learning useful behaviors [30]. Option discovery methods learn temporally-abstracted actions (i.e., options [31]), chained together to form cohesive skills [32–37]. In contrast to our work, these approaches focus on maximizing performance in single-agent settings. There also exists a related line of work for learning diverse policies in RL settings [38–46]; despite their focus on policy diversity, several of these approaches make much stronger assumptions than ours (e.g., access to the policies generating agent trajectories, or unique identifiers of the policy that generated each trajectory). By contrast, our work assumes no access to any of the underlying raw policies, or even labels of which policies agent trajectories were obtained from. Recent works have also focused on hierarchical skill learning in multiagent reinforcement learning (MARL). Lee et al. [47] use the mutual information maximization objective introduced in Eysenbach et al. [16] to learn multiagent policies. Yang et al. [48] use a bi-level policy to learn agent skills: a high-level policy first generates latent vectors for each agent,

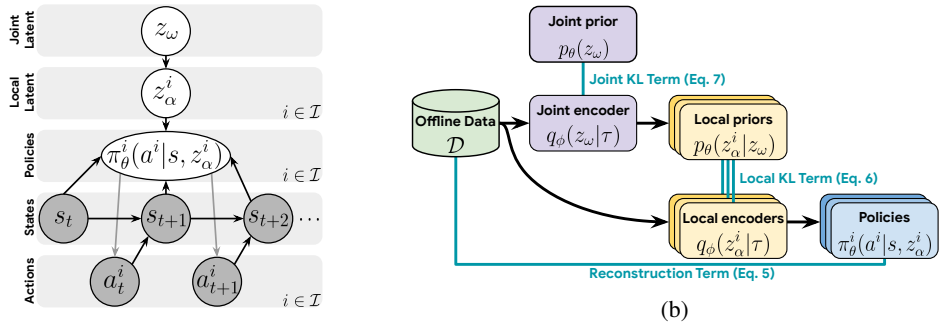

(a) (b)

Figure 2: Approach overview. (a) Graphical model of the latent-conditioned trajectory generation process that MOHBA uses to learn multiagent behavior clusters. The joint behavior latent parameter z_ω informs local (agent-wise) behavior parameters z^i_α, which affects their behavioral policies. Our approach learns these joint and local behavior spaces given a state-action trajectory dataset. (b) Architecture overview of the MOHBA model with variational lower bound terms (5) to (7) indicated.

and a low-level policy conditions behaviors on said vector to perform the task. In Wang et al. [49], distinct 'roles' are learned for agents to enable decomposition of tasks. Mao et al. [50] investigate use of consistent latent cognition variables in agent neighborhoods to induce increased cooperation. Many MARL approaches have noted the emergence of interesting behaviors in multiagent systems in specific domains of interest [51–55]. In contrast to our focus, these approaches use RL to maximize agent performance, rather than understand arbitrary behaviors via offline analysis.

RL interpretability methods primarily focus on single-agent settings and either modify the RL algorithm itself to increase transparency, or conduct post-hoc explainability [56]. These approaches represent agent policies as programming languages [57], extract visual summaries of behaviors using 'interestingness' statistics such as uncertainty in selected actions or the value of state-transitions [58], or combine agent neuron activations with gradient information to construct behavioral embeddings [59]. Behavioral clusters in our work share similarities with concept-based explanation approaches in non-RL domains. Detecting 'concepts' in pre-trained models has been explored in vision [60–62], discrete games [12], and language [63, 64]. In vision, clustering-based approaches describe discovered concepts using examples [60] or use generative modeling to create new data to describe concepts [62]. Ghorbani et al. [60] uses a vision-specific method (i.e., superpixels) to sub-divide input before conducing clustering; while sub-division is less natural in RL, our LSTM and VAE baselines serve as an RL-adopted counterpart of such works.

Works using latent-clustering and analysis are also related to ours. These include approaches using multi-level variational autoencoders [65–68] to learn compositional latent spaces, although not in decision-making domains such as ours. Hierarchical latent approaches have been used in single-agent RL [69, 70]. Behavior analysis has also been conducted by embedding agent neuron activations into a low-dimensional space, using a (non-hierarchical) variational approach [9]. The representation power of agents' internal states has also been gauged by predicting future events [11]. Overall, the key difference between the above works and ours is that our method combined hierarchical learning with behavior analysis and applies it to the multiagent setting.

3 Offline Analysis of Multiagent Behaviors

This section introduces the offline multiagent behavioral analysis problem and our proposed algorithm.

Preliminaries. We first formalize the problem of offline multiagent behavioral analysis. Consider a rewardless multiagent Markov Decision Process (MA-MDP), defined by tuple $(\mathcal{I}, \mathcal{S}, \mathcal{A}, \mathcal{T})$, where $\mathcal{I} = \{1, ..., N\}$ is the set of N agents, $\mathcal{S}$ is the state space, $\mathcal{A}$ is the action space, and $\mathcal{T}$ denotes the state transition probability function. By not relying on the presence of rewards, behaviors generated even without reliance on a reward function (e.g., human interactions, or agents using curiosity-based exploration) can be considered. We use the term 'local' for elements associated with individual agents, and 'joint' for those associated with the entire system. At each timestep $t \in \{0, \ldots, T-1\}$, the agents execute joint action $a_t \in \mathcal{A}$ in state s_t using joint policy $\pi(a_t|s_t)$, causing the state to transition to s_{t+1} with probability $p(s_{t+1}|s_t, a_t) = \mathcal{T}(s_{t+1}, a_t, s_t)$. As standard in multiagent frameworks [71],

we assume the joint action space factorizes as $\mathcal{A} = \times_i \mathcal{A}^i$, such that $a_t = (a_t^1, \ldots, a_t^N)$, where $i \in \mathcal{I}$ and $a_t^i \in \mathcal{A}^i$. Similarly, $\pi^i(a_t^i|s_t)$ is the local policy for agent i, and $\pi = \prod_i \pi^i$ is the joint policy.

Let $\tau = \big(s_0, (a_0^i)_{i\in\mathcal{I}}, \ldots, (a_{T-1}^i)_{i\in\mathcal{I}}, s_T\big)$ denote a trajectory induced by this process, and $\mathcal{D} = \{\tau_1, \ldots, \tau_K\}$ denote a dataset of K such trajectories. This dataset may consist of trajectories from multiple training runs, including variations over agent algorithms, hyperparameters, random seeds, or other factors influencing emergent behaviors. Given dataset $\mathcal{D}$, the offline multiagent analysis problem seeks to uncover potential clusters of agent behaviors.

Approach. Our approach, called the Multiagent Offline Hierarchical Behavior Analyzer (MOHBA), uses offline trajectory data to discover behaviors exhibited by agents at the local and joint level.

We first use Fig. 2a to build intuition before discussing technical details. Let the agent interactions exhibited in a trajectory τ be encoded by a latent variable, $z_\omega \in \mathbb{R}^{D_\omega}$, capturing their joint behavior. For example, z_ω may encode (at a high level) whether agents were cooperating or competing in a given trajectory; conditioned on joint signal z_ω, each agent then exhibits its own local behavior. Let local latent vectors $z_\alpha = (z_\alpha^1, \ldots, z_\alpha^N)$ encode individual agent behaviors, where $z_\alpha^i \in \mathbb{R}^{D_\alpha^i}$. Conditioned on the local behavior vector z_α^i, each agent then executes actions using a behavior-conditioned policy $\pi^i(a^i|s, z_\alpha^i)$. Given trajectory dataset $\mathcal{D}$, we seek to learn the latent-conditioned policies and distributions over latent vectors, such that we can reconstruct *any* behaviors exhibited by the agents in $\mathcal{D}$. Thus, latent vectors z_ω and z_α will encode the agents' behavioral spaces and, ideally, identify behavioral clusters in the dataset. Given this framework, the joint policy is decomposed,

$$\pi(a_t|s_t) = \int_{z_\alpha, z_\omega} \pi(a_t|s_t, z_\alpha) p(z_\alpha|z_\omega) p(z_\omega) d_{z_\alpha} d_{z_\omega} \tag{1}$$

$$= \int_{z_\alpha, z_\omega} \prod_{i=1}^{N} \pi^i(a_t^i|s_t, z_\alpha^i) p(z_\alpha^i|z_\omega) p(z_\omega) d_{z_\alpha} d_{z_\omega} \,, \tag{2}$$

where in (1) we have assumed that each agent's latent-conditioned policy is conditionally-independent of the high-level latent behavior z_ω given its low-level latent z_α^i (see Appendix A.1.1 for discussion). Next, given initial state distribution $p(s_0)$ and latent behavior spaces, the probability of a trajectory τ under joint policy $\pi(\cdot)$ is as follows:

$$p^\pi(\tau) = p(s_0) \prod_{t=0}^{T-1} p(s_{t+1}|s_t, a_t) \pi(a_t|s_t) \tag{3}$$

$$= \int_{z_\alpha, z_\omega} p(s_0) \prod_{t=0}^{T-1} p(s_{t+1}|s_t, a_t) \prod_{i=1}^{N} \pi^i(a_t^i|s_t, z_\alpha^i) p(z_\alpha^i|z_\omega) p(z_\omega) d_{z_\alpha} d_{z_\omega} \,. \tag{4}$$

We seek to learn the distributions over variables z_α and z_ω, alongside the latent-conditioned policies $\pi^i(a^i|s_t, z_\alpha^i)$, which maximize trajectory probabilities (4). In Appendix A.1, we derive the following variational lower bound, enabling approximation of these components using parametric models:

$$J_{lb} = \mathbb{E}_{\tau\sim\mathcal{D}, z_\alpha \sim q_\phi(z_\alpha|\tau)} \Big[\sum_{t,i} \log \pi_\theta^i(a_t^i|s_t, z_\alpha^i) \Big] \tag{5}$$

$$-\beta \Bigg[\mathbb{E}_{\tau\sim\mathcal{D}, z_\omega \sim q_\phi(z_\omega|\tau)} \Big[\sum_i D_{\mathrm{KL}}(q_\phi(z_\alpha^i|\tau) || p_\theta(z_\alpha^i|z_\omega)) \Big] \tag{6}$$

$$+\mathbb{E}_{\tau\sim\mathcal{D}} \left[D_{\mathrm{KL}}(q_\phi(z_\omega|\tau) || p_\theta(z_\omega)) \right] \Bigg] \,, \tag{7}$$

where $q_\phi(z_\alpha^i|\tau)$ and $p_\theta(z_\alpha^i|z_\omega)$ are, respectively, learned encoder (posterior) and prior distributions over the local behavior latents z_α^i; likewise, $q_\phi(z_\omega|\tau)$ and $p_\theta(z_\omega)$ are, respectively, learned encoder and prior distributions over the joint behavior latent z_ω; β is a KL-weighting term as in β-VAEs [72].

Figure 2b illustrates MOHBA's model architecture, which is informed by the three bound components (5) to (7). During training, each trajectory $\tau \sim \mathcal{D}$ is simultaneously passed through the joint and local encoders, which respectively produce parameters for distributions over z_ω and z_α (e.g., parameters of Gaussian distributions). Samples of low-level latent vectors z_α are passed to the

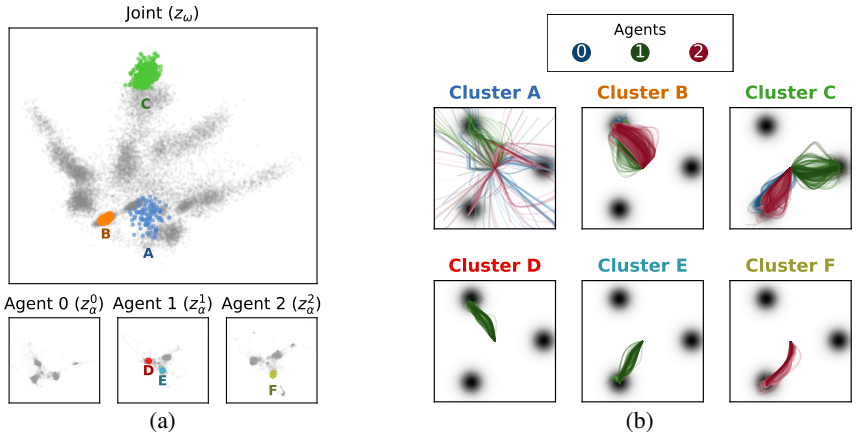

Figure 3: Results for 3-agent hill climbing domain (see interactive version here). (a) Example behavioral clusters discovered by MOHBA. (b) Trajectories corresponding to each cluster. Clusters A to C highlight joint agent behaviors, whereas D to F separately highlight those of individual agents (with other agents faded out in the latter clusters' trajectory plots for readability).

reconstructed agent policies $\pi_\theta^i(a_t^i|s_t, z_\alpha^i)$, which are trained via the reconstruction component (5). The local KL-divergence component (6) induces the local encoder distribution (which is conditioned directly on τ) to be similar to the local prior distribution (which is conditioned only on samples z_ω), thus enabling meaningful correlations between the encoded local and joint latent space, as later shown. Finally, the joint KL-divergence component (7) is akin to that in a standard variational autoencoder [73, 74]. Overall, MOHBA enables learning of a hierarchical behavioral space (at the joint and local agent levels, z_ω and z_α, respectively) that exposes interesting behavioral clusters.

4 Experiments

Our experiments showcase a variety of use-cases for MOHBA, which enrich the typical reward-centric performance monitoring used during training. Data generation, training, networks, computation resources, and hyperparameter details are provided in Appendix A.2 of the supplementary materials.

MARL data generation. Multiagent trajectory data is generated for each considered domain via the Acme RL library [75], using the TD3 algorithm [76] in a decentralized fashion, with dataset management handled using RLDS [77]. Trajectories are collected at constant intervals throughout training, which also enables analysis of behavioral emergence. We conduct a wide sweep over random seeds for data generation, yielding a diverse set of trajectories to analyze using MOHBA.

MOHBA setup. To analyze the above data using MOHBA, we use a GMM (Gaussian Mixture Model) for the joint prior, a bidirectional LSTM (long short-term memory network) with GMM head for the joint encoder, an MLP (multi-layer perceptron) with Gaussian head for the local priors, a bidirectional LSTM with Gaussian head for the local encoder, and an MLP for reconstructed policies. GMMs are used for the joint prior and encoder as they produce discernible joint behavior clusters [78], whereas the conditioning of the local prior on z_ω yields such clusters at the local level with a standard Gaussian head. We use parameter-sharing across local priors, local encoders, and reconstructed policies, as common in multiagent setups [79], with a unique one-hot vector identifier appended to agent-specific network inputs to enable heterogeneity in model outputs. We conduct a wide sweep of MOHBA hypereparameters, including the latent space dimensionality (4 and 8-dimensional), MLP hidden sizes (64 and 128 units), LSTM hidden sizes (64 and 128 units), Adam optimizer [80] learning rates (0.001 and 0.0001), with 3 seeds per parameter set (see appendix for full details).

Independent analysis of joint (z_ω) and local (z_α) behaviors. We here analyze the hierarchical latent structure learned by MOHBA. Specifically, we highlight differences in agent behaviors as identified at the joint and local levels, respectively, by z_ω and z_α. We first consider trajectories generated in a 3-agent hill-climbing domain (our earlier example in Fig. 1b). States and actions correspond, respectively, to 2D positions (x, y) and forces $(\Delta x, \Delta y)$ imparted by each agent for movement. Agents spawn at the origin and are each rewarded for climbing any of three hills within

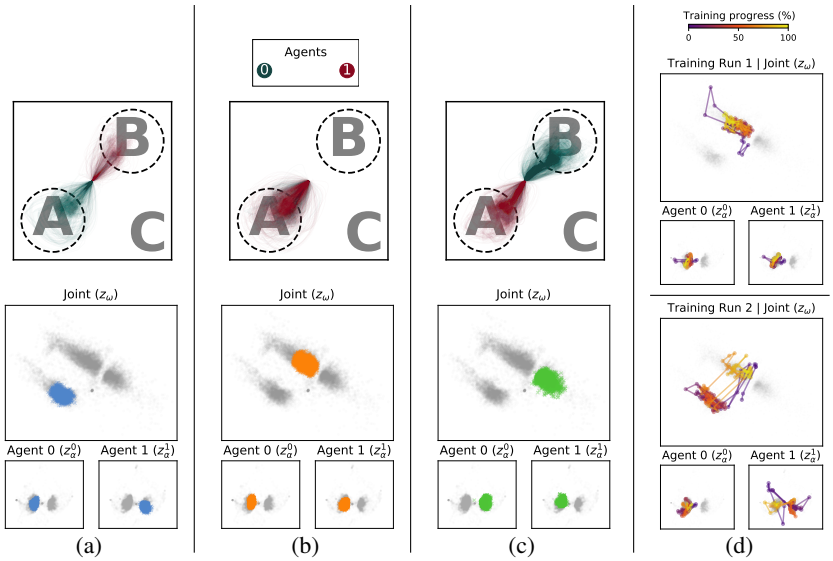

Figure 4: Results for two-agent coordination game (see interactive version here). (a) to (c) visualize key joint clusters, their corresponding local clusters for each agent, and the associated trajectories in the actual domain. (d) visualizes the progression of agent behaviors throughout the original MARL training phase, for two example training runs (top and bottom panels).

the domain in episodes of 50 timesteps (with rewards at each position indicated in Fig. 1b). We generate a dataset using 50 independent MARL training trials, each conducted for $1e5$ environment steps; trajectories are saved every 200 steps, yielding $1.25e6$ frames of data (25000 trajectories).

Figure 3a highlights several example clusters of joint and local behaviors identified by MOHBA, using samples of z_ω and z_α from the joint and local encoders. We use Euclidean distances in the original latent spaces to identify nearby vectors, then visualize their 2D projection using principal component analysis. For each cluster, we visualize all associated trajectories in Fig. 3b, thus enabling analysis of behaviors captured in latent space. Clusters A, B, and C correspond to examples of joint behaviors (z_ω). Cluster A contains trajectories early in training, where agents behave nearly randomly and have not learned to converge to a particular rewarding hill in the domain. In Cluster B, all three agents have learned to navigate towards the top-left hill. In Cluster C, agents 0 and 2 show preference for the bottom-left hill, whereas agent 1 prefers the right hill. Overall, the behavioral clusters at the joint level capture the collective behaviors of agents in a meaningful manner.

Next, we analyze individual agent clusters. Note that for all agents, three prominent clusters are apparent in their respective z_α spaces, as each training trial in the data generation process can lead to various agent-wise hill preferences. We compare two such clusters, D and E, for agent 1, observing in the trajectory plots that these corresponds to this agent preferring the top-left and bottom-left hills, respectively. Similarly, Cluster F corresponds to trajectories where agent 2 prefers the bottom-left hill. These results illustrate that the local latents reasonably disentangle each agent's observed behaviors.

Coupled analysis of joint (z_ω) and local (z_α) behaviors. The above experiments independently analyzed the joint and local latent spaces. We can also concurrently analyze them to better understand local agent contributions to joint behaviors. Consider a two-agent domain with close inter-agent coordination (visualized in the top of Fig. 4a), with state and actions-spaces similar to the hill domain and episodes consisting of 50 timesteps. Three regions are defined in this domain: A and B (circular regions), and C (region exterior to the circles). When an agent enters a given region, it 'activates' the corresponding strategy in Table 1, with agents receiving rewards at each timestep according to the joint strategy they have activated. For example, if both agents enter region A, they each receive a reward of 1, whereas if one agent enters A while the other is in exterior region C, neither receives a reward. This domain involves a significant degree of coordination as agents must discover the rewarding regions, while receiving a sparse reward signal until a valid combination of strategies is discovered. There is also

Table 1: Coordination rewards.

		Agent 1		
		A	B	C
Agent 0	A	$(1,1)$	$(1,1)$	$(0,0)$
	B	$(1,1)$	$(0,0)$	$(0,0)$
	C	$(0,0)$	$(0,0)$	$(0,0)$

potential for miscoordination: navigating to region B is rewarding assuming the other agent navigates to A, but yields 0 reward if the other agent instead navigates to B (potentially destabilizing training). We run 50 independent MARL sweeps in this domain, yielding $1e6$ data frames (20000 trajectories). As shown in Fig. 4, MOHBA discovers three dominant joint behavior clusters z_ω here. In each of Figs. 4a to 4c, we highlight one of these clusters and its corresponding local behavior latents z_α for each agent. MOHBA reveals that across the dataset, the agents have learned to cover all 3 optimal joint behaviors in Table 1: (A, A), (A, B), and (B, A). Moreover, despite each agent discovering two local behaviors (A and B), z_ω highlights only the 3 observed joint behaviors (i.e., does not simply highlight 4 clusters consisting of the Cartesian product of individual agents' behavior spaces).

Behavior emergence throughout MARL training. We next use MOHBA's latent space to inspect behavior emergence *during* MARL training. Figure 4d visualizes the training progression of two MARL runs used for data generation, tracking behavior changes throughout. In Training Run 1 (top panel of Fig. 4d), the agents converge to and maintain a fixed joint behavior throughout training. By contrast, Training Run 2 (bottom panel) has numerous behavior changepoints, where agents flip back and forth between preferring one of two clusters in z_ω. Concurrently inspecting the z_α space for Training Run 2, we observe that agent 0 converges to and maintains a consistent behavior, whereas agent 1 changes its preference sporadically, also explaining the detected changes in joint behaviors.

Baseline comparisons. We next compare against baselines previously used for multiagent behavioral analysis in the literature [9, 11]. An LSTM baseline conducts next-action prediction at each step in a trajectory τ, using an action-prediction loss (APL), defined as the $\mathcal{L}_2$ loss over predicted vs. ground truth actions. This baseline targets using the LSTM hidden states, rather than a learned distribution over latent variables, for understanding and clustering agent behaviors (akin to the analysis in [9, 11]). A flat-VAE baseline provides a non-hierarchical ablation of MOHBA that simply feeds the joint latent z_ω (rather than z^i_α) to reconstructed agent policies (i.e., $\pi^i_\theta(a^i|s, z_\omega)$); we use our usual loss (with the local KL term (6) removed) to train this VAE. We conduct a hyperparameter sweep for the baselines (see Appendix A.2), reporting the best results averaged over 3 random seeds.

Table 2: Baseline comparisons. Action-prediction loss (APL) and intra-cluster trajectory distance (ICTD); lower is better for both.

	Hill-climbing domain		Coordination game	
	APL	ICTD	APL	ICTD
LSTM	4.8 ± 0.1	0.47 ± 0.19	2.9 ± 0.1	0.34 ± 0.15
VAE	6.9 ± 0.4	$\mathbf{0.18 \pm 0.13}$	5.0 ± 0.3	$\mathbf{0.16 \pm 0.10}$
MOHBA	$\mathbf{1.3 \pm 0.1}$	$\mathbf{0.17 \pm 0.13}$	$\mathbf{2.4 \pm 0.3}$	$\mathbf{0.16 \pm 0.10}$

Comparisons are conducted at the joint behavior level: for the LSTM, we use the final hidden state as an encoding of each trajectory; for our method and the VAE, we use z_ω directly. Table 2 compares the methods in the hill-climbing and coordination game domains. Here we note the APL, which measures how well each method reconstructs ground truth policies. Additionally, we use K-means (sweeping over the # of clusters) to identify behavior clusters for each method, then report the intra-cluster trajectory distance (ICTD), defined as the average distance of all trajectories in a cluster from the mean trajectory in said cluster (akin to intra-cluster point scatter, a common cluster analysis statistic [81]) . Combined, these measures provide a proxy for evaluating the latent representations in terms of enabling accurate reconstructions (APL) while clustering similar trajectories together (ICTD). MOHBA significantly outperforms the LSTM and VAE baselines in terms of APL, while also clustering similar trajectories at the z_ω level in terms of ICTD. We provide additional results including APL throughout training, full ICTD sweeps, and visualizations of the latent spaces for the baselines in Appendix A.3.2.

Behavior concept discovery. Next, we test the representation power of the latent spaces learned by MOHBA, and illustrate a means of discovering 'behavior concepts' in the latent space. We adopt the completeness-aware concept explanations framework of Yeh et al. [13], with slight changes to make it amenable to this setting (see Appendix A.2.5). At a high-level, given a set of inputs, a set of concept vectors C in the same space as inputs, and prediction targets (e.g., domain characteristics of interest), Yeh et al. [13] define a framework to compute class-conditioned Shapley values, called ConceptSHAP. To do so, every input is projected onto each of the concept vectors, yielding a vector of 'concept scores', which is then passed to a simple prediction head g (e.g., small MLP or linear model) to predict the targets and compute the ConceptSHAP. ConceptSHAP provides numerical scores interpreted as the importance of each concept in C for predicting a given target class, which is useful for identifying key concepts (and nearby inputs) associated with certain domain characteristics.

Table 3: Discovered concepts using z_ω in hill-climbing domain. For each characteristic (agent dispersion and return), 5 classes are constructed using the ground truth information in trajectories τ. The concept explanation framework of Yeh et al. [13] is then used to first predict the correct classes (using only z_ω, rather than the trajectory τ, as input), then identify core concepts related to each class.

Concept	Top discovered concept using z_ω (per class, with average concept measure beneath)				
	Class 0	Class 1	Class 2	Class 3	Class 4
Agent Dispersion (Classification accuracy: 54.27%)	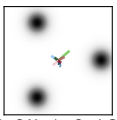 0.05 ± 0.13	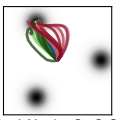 0.15 ± 0.06	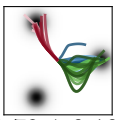 1.79 ± 0.10	2.18 ± 0.19	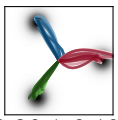 2.36 ± 0.10
Total Return (Classification accuracy: 60.98%)	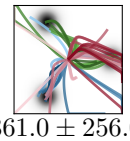 361.0 ± 256.0	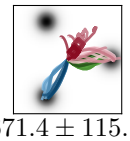 671.4 ± 115.1	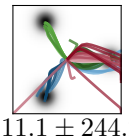 611.1 ± 244.2	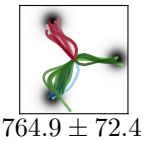 764.9 ± 72.4	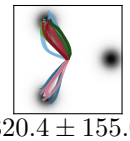 820.4 ± 155.0

In Table 3, we use this technique to identify behavioral concepts in z_ω space associated with several characteristics of interest in the hill-climbing domain. The set of concepts C we consider are generated using K-means in the z_ω space (see Appendix A.2.5 for details), and a simple 2-layer MLP with 8-hidden units for prediction head g. The first row of Table 3 shows classes corresponding to increasing levels of agent dispersion in the domain (with dispersion defined as the sum of $\mathcal{L}_2$-distances of agents from their centroid at the final timestep of the episode). For each trajectory τ, we compute the associated dispersion, creating 5 classes of equal-sized bins (with labels 0 through 4 mapping to bins of increasing dispersion). We create a train-validation split of 80-20, then train the MLP g via a softmax-cross entropy loss to predict the correct classes using only z_ω as input (rather than the actual trajectory τ). We attain a validation set accuracy of 54.27%, signifying the predictive capabilities of z_ω. Next, we compute the class-conditioned ConceptSHAP, thus identifying the top-scoring concept vector for each class. In Table 3, we visualize the 20 trajectories with the closest z_ω to the top-scoring concept for each class (with the mean agent dispersion across these trajectories listed under each image). Intuitively, the identified concepts involve agents becoming increasingly dispersed, with agents first nearly stationary at the center (class 0), then all converging to the same hill (class 1), spreading across two hills (class 2), and finally covering all hills (classes 3 and 4).

The second row of Table 3 repeats the same experiment, now using classes associated with the sum of returns of agents. We attain a validation set accuracy of 60.98%, and similarly observe behavioral trajectories associated with generally increasing reward by identifying top clusters for each class (with some overlaps, e.g., classes 1 and 2 with high standard deviation in returns). Overall, this line of experiments provides both a means of quantifying the representational capacity of z_ω, and also of identifying clusters of concepts associated with certain behavioral characteristics.

Scalability to high-dimensional domains. We next test MOHBA's scalability to high-dimensional domains using the 2-Agent HalfCheetah multiagent MuJoCo domain [14], where agents 0 and 1, respectively, control the back and front limbs of a cheetah to coordinate movement. Each agent's state consists of a 6D vector summarizing velocity and position information for the 3 joints it controls, with its 3D action space corresponding to motor torques applied to said joints. The agents coordinate to maximize the forward-speed of the cheetah over episodes of 200 timesteps each. We generate data using 30 independent trials of MARL training, collecting $1e5$ total trajectories to train MOHBA.

Figure 5a visualizes the behavior space learned by MOHBA, wherein we observe several clusters. We highlight three example trajectories stemming from distinct clusters in the joint behavior space z_ω, showing the corresponding HalfCheetah behaviors in Fig. 5b. The left panel of each example provides a view of the cheetah's overall movement, where we observe key behavior differences: in Example A, the cheetah runs forward using subtle vibration of its limbs; in Example B, it bounces forward with its torso arched up due to its front limb (agent 1) being more extended than its back limb (agent 0); in Example C, it moves closer to the ground with its torso arched down. In the latent space (Fig. 5a), we observe that for Examples B and C, the z_α^0 (back limb) latents are close to one another, while the z_α^1 (front limb) latents are far apart. To investigate these local agent behavioral differences,

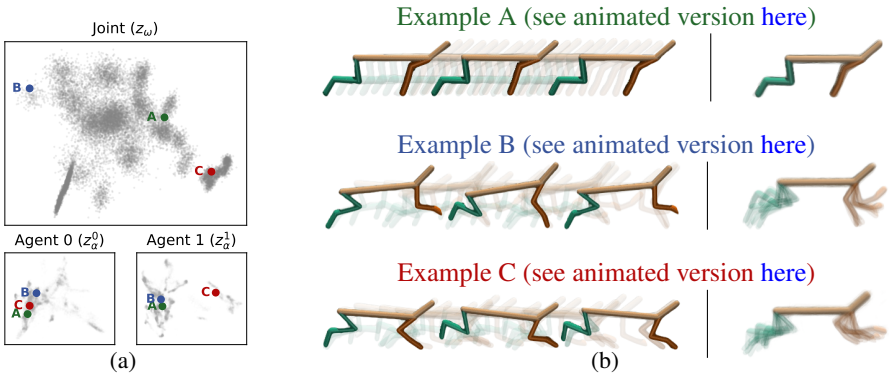

Figure 5: Multiagent MuJoCo HalfCheetah behavioral space (see interactive version here). Agent 0 and 1, respectively, control the back and front limbs, coordinating to move the cheetah. (a) Detected behavioral space, with three example trajectories indicated. (b) HalfCheetah behavior corresponding to the same three examples (left panels showing trajectory frames, and right panels showing the same frames with the cheetah torso aligned to disambiguate the back and front leg agent behaviors).

the right panel of Fig. 5b provides an overlaid view of the same frames, with the torso now aligned (making it easier to discern the behaviors of agent 0 vs. agent 1). Here we observe that the back limb (agent 0) behaves similarly across both examples, while the front limb (agent 1) stays much closer to the head for Example C, in contrast to Example B, which coincides with the findings in the z_α space.

5 Discussion

Our proposed method, MOHBA, leverages trajectory data to better understand multiagent behaviors during and after training. MOHBA assumes no knowledge of agents' underlying training algorithms, does not require access to their hidden states or internal models, and applies even to reward-free settings. Our experiments showcased a variety of applications of MOHBA, including the analysis of joint and local agent behaviors, monitoring of behavior emergence throughout training, discovery of behavioral concepts associated with certain domain criteria, and disentanglement of behaviors stemming from externally-available open-source policies such as those for OpenAI hide-and-seek [10].

While we believe our approach is an important step in terms of increasing the understanding of multiagent systems, there are several limitations and potential societal impacts of note. One limitation is related to the collection of a dataset of agent behaviors. By collecting this dataset throughout agent training, we ensure that the most prominent behaviors that can occur in a given environment can be identified using our method. However, this requires both storage of larger datasets than usual agent training requires, and also the use of a large enough sweep of agent training to capture key behaviors. It may be interesting to consider follow-ups to our model that learn behavioral clusters in a streaming fashion, thus building knowledge of behaviors over time and permitting older data to be discarded throughout agent training. Moreover, in our datasets, we collected trajectories at uniform intervals throughout original MARL training. However, it might be interesting to consider a scheme that does so in a non-uniform manner; this can be done in a variety of ways (e.g., using a pre-trained MOHBA model to detect divergences from previously-seen behaviors during future MARL training runs, and collecting trajectories only when such divergences occur). Finally, it might be interesting to enable the agents to first learn joint behaviors / 'skills' using the proposed method, and leverage them to transfer to related downstream tasks (potentially more sample-efficiently than training from scratch).

Moreover, the study of behavioral interactions in multiagent systems can potentially be used for both positive and negative societal applications. For example, such an approach could be used to prevent certain undesirable behaviors by agents that interact with humans (e.g, self-driving cars), but potentially also used by adversaries to predict and exploit other behaviors (e.g., exploiting certain human preferences for harm), or even inadvertently cause harm due to misinterpretation of certain behavioral modes. As such, further research and evaluation will be required prior to deployment of this and related behavioral analysis approaches to human-facing domains. Nonetheless, as agent capabilities continue to grow, our view is that behavioral analysis of multiagent systems will become increasingly important and should complement traditional reward-based performance monitoring.

References

[1] Gerald Tesauro et al. Temporal difference learning and TD-gammon. *Communications of the ACM*, 38(3):58–68, 1995.

[2] Murray Campbell, A Joseph Hoane Jr, and Feng-hsiung Hsu. Deep blue. *Artificial intelligence*, 134(1-2):57–83, 2002.

[3] David Silver, Aja Huang, Chris J Maddison, Arthur Guez, Laurent Sifre, George Van Den Driessche, Julian Schrittwieser, Ioannis Antonoglou, Veda Panneershelvam, Marc Lanctot, et al. Mastering the game of go with deep neural networks and tree search. *nature*, 529(7587):484–489, 2016.

[4] David Silver, Thomas Hubert, Julian Schrittwieser, Ioannis Antonoglou, Matthew Lai, Arthur Guez, Marc Lanctot, Laurent Sifre, Dharshan Kumaran, Thore Graepel, et al. A general reinforcement learning algorithm that masters chess, shogi, and go through self-play. *Science*, 362(6419):1140–1144, 2018.

[5] Noam Brown and Tuomas Sandholm. Superhuman ai for heads-up no-limit poker: Libratus beats top professionals. *Science*, 359(6374):418–424, 2018.

[6] Oriol Vinyals, Igor Babuschkin, Wojciech M Czarnecki, Michaël Mathieu, Andrew Dudzik, Junyoung Chung, David H Choi, Richard Powell, Timo Ewalds, Petko Georgiev, et al. Grandmaster level in starcraft ii using multi-agent reinforcement learning. *Nature*, 575(7782):350–354, 2019.

[7] Christopher Berner, Greg Brockman, Brooke Chan, Vicki Cheung, Przemysław Dębiak, Christy Dennison, David Farhi, Quirin Fischer, Shariq Hashme, Chris Hesse, et al. Dota 2 with large scale deep reinforcement learning. *arXiv preprint arXiv:1912.06680*, 2019.

[8] Noam Brown and Tuomas Sandholm. Superhuman ai for multiplayer poker. *Science*, 365 (6456):885–890, 2019.

[9] Max Jaderberg, Wojciech M Czarnecki, Iain Dunning, Luke Marris, Guy Lever, Antonio Garcia Castaneda, Charles Beattie, Neil C Rabinowitz, Ari S Morcos, Avraham Ruderman, et al. Human-level performance in 3D multiplayer games with population-based reinforcement learning. *Science*, 364(6443):859–865, 2019.

[10] Bowen Baker, Ingmar Kanitscheider, Todor Markov, Yi Wu, Glenn Powell, Bob McGrew, and Igor Mordatch. Emergent tool use from multi-agent autocurricula. In *International Conference on Learning Representations*, 2020. URL `https://openreview.net/forum?id=SkxpxJBKwS`.

[11] Siqi Liu, Guy Lever, Zhe Wang, Josh Merel, SM Eslami, Daniel Hennes, Wojciech M Czarnecki, Yuval Tassa, Shayegan Omidshafiei, Abbas Abdolmaleki, et al. From motor control to team play in simulated humanoid football. *arXiv preprint arXiv:2105.12196*, 2021.

[12] Thomas McGrath, Andrei Kapishnikov, Nenad Tomasev, Adam Pearce, Demis Hassabis, Been Kim, Ulrich Paquet, and Vladimir Kramnik. Acquisition of chess knowledge in alphazero. *CoRR*, abs/2111.09259, 2021. URL `https://arxiv.org/abs/2111.09259`.

[13] Chih-Kuan Yeh, Been Kim, Sercan Arik, Chun-Liang Li, Tomas Pfister, and Pradeep Ravikumar. On completeness-aware concept-based explanations in deep neural networks. *Advances in Neural Information Processing Systems*, 33:20554–20565, 2020.

[14] Christian Schröder de Witt, Bei Peng, Pierre-Alexandre Kamienny, Philip HS Torr, Wendelin Böhmer, and Shimon Whiteson. Deep multi-agent reinforcement learning for decentralized continuous cooperative control. 2020.

[15] Özgür Şimşek and Andrew Barto. Skill characterization based on betweenness. *Advances in neural information processing systems*, 21, 2008.

[16] Benjamin Eysenbach, Abhishek Gupta, Julian Ibarz, and Sergey Levine. Diversity is all you need: Learning skills without a reward function. In *International Conference on Learning Representations*, 2018.

[17] Karol Hausman, Jost Tobias Springenberg, Ziyu Wang, Nicolas Heess, and Martin Riedmiller. Learning an embedding space for transferable robot skills. In *International Conference on Learning Representations*, 2018.

[18] Thomas Kipf, Yujia Li, Hanjun Dai, Vinicius Zambaldi, Alvaro Sanchez-Gonzalez, Edward Grefenstette, Pushmeet Kohli, and Peter Battaglia. Compile: Compositional imitation learning and execution. In *International Conference on Machine Learning*, pages 3418–3428. PMLR, 2019.

[19] Archit Sharma, Shixiang Gu, Sergey Levine, Vikash Kumar, and Karol Hausman. Dynamics-aware unsupervised discovery of skills. In *International Conference on Learning Representations*, 2019.

[20] Leonard Hasenclever, Fabio Pardo, Raia Hadsell, Nicolas Heess, and Josh Merel. Comic: Complementary task learning & mimicry for reusable skills. In *International Conference on Machine Learning*, pages 4105–4115. PMLR, 2020.

[21] Corey Lynch, Mohi Khansari, Ted Xiao, Vikash Kumar, Jonathan Tompson, Sergey Levine, and Pierre Sermanet. Learning latent plans from play. In *Conference on robot learning*, pages 1113–1132. PMLR, 2020.

[22] Avi Singh, Huihan Liu, Gaoyue Zhou, Albert Yu, Nicholas Rhinehart, and Sergey Levine. Parrot: Data-driven behavioral priors for reinforcement learning. In *International Conference on Learning Representations*, 2020.

[23] Tanmay Shankar and Abhinav Gupta. Learning robot skills with temporal variational inference. In *International Conference on Machine Learning*, pages 8624–8633. PMLR, 2020.

[24] Víctor Campos, Alexander Trott, Caiming Xiong, Richard Socher, Xavier Giró-i Nieto, and Jordi Torres. Explore, discover and learn: Unsupervised discovery of state-covering skills. In *International Conference on Machine Learning*, pages 1317–1327. PMLR, 2020.

[25] Karl Pertsch, Youngwoon Lee, and Joseph Lim. Accelerating reinforcement learning with learned skill priors. In *Conference on Robot Learning*, pages 188–204. PMLR, 2021.

[26] Kate Baumli, David Warde-Farley, Steven Hansen, and Volodymyr Mnih. Relative variational intrinsic control. In *Proceedings of the AAAI Conference on Artificial Intelligence*, volume 35, pages 6732–6740, 2021.

[27] Valentin Villecroze, Harry J Braviner, Panteha Naderian, Chris J Maddison, and Gabriel Loaiza-Ganem. Bayesian nonparametrics for offline skill discovery. *arXiv preprint arXiv:2202.04675*, 2022.

[28] Yifeng Zhu, Peter Stone, and Yuke Zhu. Bottom-up skill discovery from unsegmented demonstrations for long-horizon robot manipulation. *IEEE Robotics and Automation Letters*, 2022.

[29] Tanmay Shankar, Shubham Tulsiani, Lerrel Pinto, and Abhinav Gupta. Discovering motor programs by recomposing demonstrations. In *International Conference on Learning Representations*, 2019.

[30] Anurag Ajay, Aviral Kumar, Pulkit Agrawal, Sergey Levine, and Ofir Nachum. Opal: Offline primitive discovery for accelerating offline reinforcement learning. In *International Conference on Learning Representations*, 2020.

[31] Richard S Sutton, Doina Precup, and Satinder Singh. Between mdps and semi-mdps: A framework for temporal abstraction in reinforcement learning. *Artificial intelligence*, 112(1-2): 181–211, 1999.

[32] Aravind Srinivas, Ramnandan Krishnamurthy, Peeyush Kumar, and Balaraman Ravindran. Option discovery in hierarchical reinforcement learning using spatio-temporal clustering. *arXiv preprint arXiv:1605.05359*, 2016.

[33] Peter Henderson, Wei-Di Chang, Pierre-Luc Bacon, David Meger, Joelle Pineau, and Doina Precup. Optiongan: Learning joint reward-policy options using generative adversarial inverse reinforcement learning. In *Proceedings of the AAAI conference on artificial intelligence*, volume 32, 2018.

[34] Joshua Achiam, Harrison Edwards, Dario Amodei, and Pieter Abbeel. Variational option discovery algorithms. *arXiv preprint arXiv:1807.10299*, 2018.

[35] André Barreto, Diana Borsa, Shaobo Hou, Gheorghe Comanici, Eser Aygün, Philippe Hamel, Daniel Toyama, Shibl Mourad, David Silver, Doina Precup, et al. The option keyboard: Combining skills in reinforcement learning. *Advances in Neural Information Processing Systems*, 32, 2019.

[36] Arjun Manoharan, Rahul Ramesh, and Balaraman Ravindran. Option encoder: A framework for discovering a policy basis in reinforcement learning. In *Joint European Conference on Machine Learning and Knowledge Discovery in Databases*, pages 509–524. Springer, 2020.

[37] Jaekyeom Kim, Seohong Park, and Gunhee Kim. Unsupervised skill discovery with bottleneck option learning. In *International Conference on Machine Learning*, pages 5572–5582. PMLR, 2021.

[38] Andrei Lupu, Brandon Cui, Hengyuan Hu, and Jakob Foerster. Trajectory diversity for zero-shot coordination. In *International Conference on Machine Learning*, pages 7204–7213. PMLR, 2021.

[39] Jack Parker-Holder, Aldo Pacchiano, Krzysztof M Choromanski, and Stephen J Roberts. Effective diversity in population based reinforcement learning. *Advances in Neural Information Processing Systems*, 33:18050–18062, 2020.

[40] Zihan Zhou, Wei Fu, Bingliang Zhang, and Yi Wu. Continuously discovering novel strategies via reward-switching policy optimization. In *International Conference on Learning Representations*, 2021.

[41] Justin K Pugh, Lisa B Soros, and Kenneth O Stanley. Quality diversity: A new frontier for evolutionary computation. *Frontiers in Robotics and AI*, page 40, 2016.

[42] Zhenggang Tang, Chao Yu, Boyuan Chen, Huazhe Xu, Xiaolong Wang, Fei Fang, Simon Du, Yu Wang, and Yi Wu. Discovering diverse multi-agent strategic behavior via reward randomization. *arXiv preprint arXiv:2103.04564*, 2021.

[43] Yuhang Song, Jianyi Wang, Thomas Lukasiewicz, Zhenghua Xu, and Mai Xu. Diversity-driven extensible hierarchical reinforcement learning. In *Proceedings of the AAAI conference on artificial intelligence*, volume 33, pages 4992–4999, 2019.

[44] Zhang-Wei Hong, Tzu-Yun Shann, Shih-Yang Su, Yi-Hsiang Chang, Tsu-Jui Fu, and Chun-Yi Lee. Diversity-driven exploration strategy for deep reinforcement learning. *Advances in neural information processing systems*, 31, 2018.

[45] Tanmay Gangwani, Qiang Liu, and Jian Peng. Learning self-imitating diverse policies. In *International Conference on Learning Representations*, 2018.

[46] Andrew Cohen, Xingye Qiao, Lei Yu, Elliot Way, and Xiangrong Tong. Diverse exploration via conjugate policies for policy gradient methods. In *Proceedings of the AAAI Conference on Artificial Intelligence*, volume 33, pages 3404–3411, 2019.

[47] Youngwoon Lee, Jingyun Yang, and Joseph J Lim. Learning to coordinate manipulation skills via skill behavior diversification. In *International Conference on Learning Representations*, 2019.

[48] Jiachen Yang, Igor Borovikov, and Hongyuan Zha. Hierarchical cooperative multi-agent reinforcement learning with skill discovery. In *Proceedings of the 19th International Conference on Autonomous Agents and MultiAgent Systems*, pages 1566–1574, 2020.

[49] Tonghan Wang, Tarun Gupta, Anuj Mahajan, Bei Peng, Shimon Whiteson, and Chongjie Zhang. Rode: Learning roles to decompose multi-agent tasks. In *International Conference on Learning Representations*, 2020.

[50] Hangyu Mao, Wulong Liu, Jianye Hao, Jun Luo, Dong Li, Zhengchao Zhang, Jun Wang, and Zhen Xiao. Neighborhood cognition consistent multi-agent reinforcement learning. In *Proceedings of the AAAI conference on artificial intelligence*, volume 34, pages 7219–7226, 2020.

[51] Michael Bradley Johanson, Edward Hughes, Finbarr Timbers, and Joel Z. Leibo. Emergent bartering behaviour in multi-agent reinforcement learning, 2022. URL `https://arxiv.org/abs/2205.06760`.

[52] Kris Cao, Angeliki Lazaridou, Marc Lanctot, Joel Z Leibo, Karl Tuyls, and Stephen Clark. Emergent communication through negotiation. In *International Conference on Learning Representations*, 2018.

[53] Michael Noukhovitch, Travis LaCroix, Angeliki Lazaridou, and Aaron Courville. Emergent communication under competition. In *Proceedings of the 20th International Conference on Autonomous Agents and MultiAgent Systems*, pages 974–982, 2021.

[54] Siqi Liu, Guy Lever, Josh Merel, Saran Tunyasuvunakool, Nicolas Heess, and Thore Graepel. Emergent coordination through competition. In *International Conference on Learning Representations*, 2018.

[55] Trapit Bansal, Jakub Pachocki, Szymon Sidor, Ilya Sutskever, and Igor Mordatch. Emergent complexity via multi-agent competition. In *International Conference on Learning Representations*, 2018.

[56] Alexandre Heuillet, Fabien Couthouis, and Natalia Díaz-Rodríguez. Explainability in deep reinforcement learning. *Knowledge-Based Systems*, 214:106685, 2021.

[57] Abhinav Verma, Vijayaraghavan Murali, Rishabh Singh, Pushmeet Kohli, and Swarat Chaudhuri. Programmatically interpretable reinforcement learning. In *International Conference on Machine Learning*, pages 5045–5054. PMLR, 2018.

[58] Pedro Sequeira and Melinda Gervasio. Interestingness elements for explainable reinforcement learning: Understanding agents' capabilities and limitations. *Artificial Intelligence*, 288:103367, 2020.

[59] Tom Zahavy, Nir Ben-Zrihem, and Shie Mannor. Graying the black box: Understanding dqns. In *International Conference on Machine Learning*, pages 1899–1908. PMLR, 2016.

[60] Amirata Ghorbani, James Wexler, James Zou, and Been Kim. Towards automatic concept-based explanations. *arXiv preprint arXiv:1902.03129*, 2019.

[61] David Bau, Jun-Yan Zhu, Hendrik Strobelt, Agata Lapedriza, Bolei Zhou, and Antonio Torralba. Understanding the role of individual units in a deep neural network. *Proceedings of the National Academy of Sciences*, 2020. ISSN 0027-8424. doi: 10.1073/pnas.1907375117. URL `https://www.pnas.org/content/early/2020/08/31/1907375117`.

[62] Asma Ghandeharioun, Been Kim, Chun-Liang Li, Brendan Jou, Brian Eoff, and Rosalind W. Picard. DISSECT: disentangled simultaneous explanations via concept traversals. *CoRR*, abs/2105.15164, 2021. URL `https://arxiv.org/abs/2105.15164`.

[63] Anna Rogers, Olga Kovaleva, and Anna Rumshisky. A primer in bertology: What we know about how BERT works. *CoRR*, abs/2002.12327, 2020. URL `https://arxiv.org/abs/2002.12327`.

[64] John Hewitt and Christopher D. Manning. A structural probe for finding syntax in word representations. In *Proceedings of the 2019 Conference of the North American Chapter of the Association for Computational Linguistics: Human Language Technologies, Volume 1 (Long and Short Papers)*, pages 4129–4138, Minneapolis, Minnesota, June 2019. Association for Computational Linguistics. doi: 10.18653/v1/N19-1419. URL `https://aclanthology.org/N19-1419`.

[65] Diane Bouchacourt, Ryota Tomioka, and Sebastian Nowozin. Multi-level variational autoencoder: Learning disentangled representations from grouped observations. In *Proceedings of the AAAI Conference on Artificial Intelligence*, volume 32, 2018.

[66] Arash Vahdat and Jan Kautz. Nvae: A deep hierarchical variational autoencoder. *Advances in Neural Information Processing Systems*, 33:19667–19679, 2020.

[67] Dinghan Shen, Asli Celikyilmaz, Yizhe Zhang, Liqun Chen, Xin Wang, Jianfeng Gao, and Lawrence Carin. Towards generating long and coherent text with multi-level latent variable models. In *ACL 2019-57th Annual Meeting of the Association for Computational Linguistics, Proceedings of the Conference*, pages 2079–2089. Association for Computational Linguistics (ACL), 2020.

[68] Rewon Child. Very deep vaes generalize autoregressive models and can outperform them on images. In *International Conference on Learning Representations*, 2020.

[69] Tuomas Haarnoja, Kristian Hartikainen, Pieter Abbeel, and Sergey Levine. Latent space policies for hierarchical reinforcement learning. In *International Conference on Machine Learning*, pages 1851–1860. PMLR, 2018.

[70] Dushyant Rao, Fereshteh Sadeghi, Leonard Hasenclever, Markus Wulfmeier, Martina Zambelli, Giulia Vezzani, Dhruva Tirumala, Yusuf Aytar, Josh Merel, Nicolas Heess, et al. Learning transferable motor skills with hierarchical latent mixture policies. In *Deep RL Workshop NeurIPS 2021*, 2021.

[71] Frans A Oliehoek and Christopher Amato. *A concise introduction to decentralized POMDPs*. Springer, 2016.

[72] Irina Higgins, Loic Matthey, Arka Pal, Christopher Burgess, Xavier Glorot, Matthew Botvinick, Shakir Mohamed, and Alexander Lerchner. beta-vae: Learning basic visual concepts with a constrained variational framework. In *International Conference on Machine Learning*, 2017.

[73] Diederik P Kingma and Max Welling. Auto-encoding variational bayes. In *International Conference on Learning Representations*, 2014.

[74] Danilo Jimenez Rezende, Shakir Mohamed, and Daan Wierstra. Stochastic backpropagation and approximate inference in deep generative models. In *International conference on machine learning*, pages 1278–1286. PMLR, 2014.

[75] Matt Hoffman, Bobak Shahriari, John Aslanides, Gabriel Barth-Maron, Feryal Behbahani, Tamara Norman, Abbas Abdolmaleki, Albin Cassirer, Fan Yang, Kate Baumli, Sarah Henderson, Alex Novikov, Sergio Gómez Colmenarejo, Serkan Cabi, Caglar Gulcehre, Tom Le Paine, Andrew Cowie, Ziyu Wang, Bilal Piot, and Nando de Freitas. Acme: A research framework for distributed reinforcement learning. *arXiv preprint arXiv:2006.00979*, 2020.

[76] Scott Fujimoto, Herke Hoof, and David Meger. Addressing function approximation error in actor-critic methods. In *International conference on machine learning*, pages 1587–1596. PMLR, 2018.

[77] Sabela Ramos, Sertan Girgin, Léonard Hussenot, Damien Vincent, Hanna Yakubovich, Daniel Toyama, Anita Gergely, Piotr Stanczyk, Raphael Marinier, Jeremiah Harmsen, Olivier Pietquin, and Nikola Momchev. RLDS: an ecosystem to generate, share and use datasets in reinforcement learning. *arXiv preprint arXiv:2111.02767*, 2021.

[78] Zhuxi Jiang, Yin Zheng, Huachun Tan, Bangsheng Tang, and Hanning Zhou. Variational deep embedding: An unsupervised and generative approach to clustering. In *Proceedings of the Twenty-Sixth International Joint Conference on Artificial Intelligence, IJCAI-17*, pages 1965–1972, 2017.

[79] Filippos Christianos, Georgios Papoudakis, Muhammad A Rahman, and Stefano V Albrecht. Scaling multi-agent reinforcement learning with selective parameter sharing. In *International Conference on Machine Learning*, pages 1989–1998. PMLR, 2021.

[80] Diederik P Kingma and Jimmy Ba. Adam: A method for stochastic optimization. *arXiv preprint arXiv:1412.6980*, 2014.

[81] Trevor Hastie, Robert Tibshirani, Jerome H Friedman, and Jerome H Friedman. *The elements of statistical learning: data mining, inference, and prediction*, volume 2. Springer, 2009.

[82] Xiaodong Liu Jianfeng Gao Asli Celikyilmaz Lawrence Carin Hao Fu, Chunyuan Li. Cyclical annealing schedule: A simple approach to mitigating KL vanishing. In *NAACL*, 2019.

[83] Scott M Lundberg and Su-In Lee. A unified approach to interpreting model predictions. *Advances in neural information processing systems*, 30, 2017.

[84] Justin Fu, Aviral Kumar, Ofir Nachum, George Tucker, and Sergey Levine. D4rl: Datasets for deep data-driven reinforcement learning. *arXiv preprint arXiv:2004.07219*, 2020.

Checklist

1. For all authors...
   (a) Do the main claims made in the abstract and introduction accurately reflect the paper's contributions and scope? [Yes]
   (b) Did you describe the limitations of your work? [Yes] We include these in the Discussions section.
   (c) Did you discuss any potential negative societal impacts of your work? [Yes] We include these in the discussions section.
   (d) Have you read the ethics review guidelines and ensured that your paper conforms to them? [Yes]
2. If you are including theoretical results...
   (a) Did you state the full set of assumptions of all theoretical results? [Yes] These are provided in the main paper and the proofs included in the appendix.
   (b) Did you include complete proofs of all theoretical results? [Yes] Proofs are provided in the appendix.
3. If you ran experiments...
   (a) Did you include the code, data, and instructions needed to reproduce the main experimental results (either in the supplemental material or as a URL)? [No] We provide details for experiment reproducibility in Appendix A.2. We intend to include code for the model upon paper acceptance.
   (b) Did you specify all the training details (e.g., data splits, hyperparameters, how they were chosen)? [Yes] We provide all training details in Appendix A.2.
   (c) Did you report error bars (e.g., with respect to the random seed after running experiments multiple times)? [Yes]
   (d) Did you include the total amount of compute and the type of resources used (e.g., type of GPUs, internal cluster, or cloud provider)? [Yes] We provide all computational details in Appendix A.2.
4. If you are using existing assets (e.g., code, data, models) or curating/releasing new assets...
   (a) If your work uses existing assets, did you cite the creators? [N/A] Our work does not use existing assets.
   (b) Did you mention the license of the assets? [N/A] Our work does not use existing assets.
   (c) Did you include any new assets either in the supplemental material or as a URL? [No]
   (d) Did you discuss whether and how consent was obtained from people whose data you're using/curating? [N/A] Our work does not use existing assets.
   (e) Did you discuss whether the data you are using/curating contains personally identifiable information or offensive content? [N/A] Our work does not use existing assets.
5. If you used crowdsourcing or conducted research with human subjects...
   (a) Did you include the full text of instructions given to participants and screenshots, if applicable? [N/A] Our work does not crowdsourced or human subject data.

(b) Did you describe any potential participant risks, with links to Institutional Review Board (IRB) approvals, if applicable? [N/A] Our work does not crowdsourced or human subject data.

(c) Did you include the estimated hourly wage paid to participants and the total amount spent on participant compensation? [N/A] Our work does not crowdsourced or human subject data.

A Appendix for 'Beyond Rewards: a Hierarchical Perspective on Offline Multiagent Behavioral Analysis'

A.1 Derivations

A.1.1 On the Conditional Independence of π^i from z_ω given z^i_α

In (1), we assumed that each agent's latent-conditioned policy is conditionally-independent of the high-level latent behavior z_ω given its low-level latent z^i_α. This section provides some justification of this assumption.

One of the prototypical paradigms in multiagent (MARL) training is that of 'centralized training, decentralized execution'. In this regime, each agent's decision-making policy is conditioned only on its available local information / local observations during execution; thus, the behaviors exhibited by each agent are ultimately informed by their local information, rather than global (joint) information.

In our setting, z^i_α serves to provide this local behavior context for each agent. Thus, the assumption of the policy being conditionally-independent of z_ω given z^i_α corresponds well to the assumption of agents only using local information (rather than joint information) in MARL to inform their policy/decision-making.

Nonetheless, we also note that there is a strong relationship between local and joint behaviors in our setting, which provides a coordination signal to the policy implicitly through z^i_α. Specifically, our derivation results in a local behavior prior term, $p(z^i_\alpha|z_\omega)$; using this term, the joint behavior latent z_ω is able to influence the learned space over local behavior latents z^i_α. Thus, the information-flow in our framework can be more intuitively described as follows:

1. The joint behavior latent observes a trajectory and summarizes the joint behavior exhibited in it (e.g., team-wide cooperation, competition, etc.) in z_ω
2. Subsequently, this joint latent z_ω affects the space of z^i_α, which are then sampled and used to inform each agent how to behave locally in order to achieve the joint behavior observed.

Overall, the above relationship between the two latent spaces implies makes the conditional-independence of the policy from z_ω a reasonable simplifying assumption.

A.1.2 Derivation of the Variational Lower Bound

This section details the derivation of the variational lower bound described in Section 3 of the main text, which is used for training MOHBA.

Similar to traditional variational autoencoder approaches [73, 74], we approximate the maximization of the latent-conditioned trajectory probability (4) in the main text using the evidence lower bound

$$J_{lb} = \mathbb{E}_{\tau\sim\mathcal{D},q_\phi(z_\alpha,z_\omega|\tau)}\left[\log p^\pi(\tau|z_\alpha,z_\omega)\right] - \mathbb{E}_{\tau\sim\mathcal{D}}[D_{\mathrm{KL}}(q_\phi(z_\alpha,z_\omega|\tau)||p_\theta(z_\alpha,z_\omega))]\ , \tag{8}$$

where $q_\phi(\cdot|\tau)$ and $p_\theta(\cdot)$ are, respectively, learned posterior and prior distributions.

Using (4) from the main text to expand this expression yields

$$\begin{aligned} J_{lb} = \mathbb{E}_{\tau\sim\mathcal{D},q_\phi(z_\alpha,z_\omega|\tau)}&\left[\log p(s_0) + \sum_t \log p(s_{t+1}|s_t,a_t) + \sum_{t,i}\log \pi^i_\theta(a^i_t|s_t,z^i_\alpha)\right] \\ &- \mathbb{E}_{\tau\sim\mathcal{D}}\left[D_{\mathrm{KL}}(q_\phi(z_\alpha,z_\omega|\tau)||p_\theta(z_\alpha,z_\omega))\right] \end{aligned} \tag{9}$$

Note that the terms $p(s_0)$ and $p(s_{t+1}|s_t,a_t)$ stem from the underlying MA-MDP environment, and thus cannot be optimized via parameters ϕ and θ. Dropping these extraneous terms yields,

$$J_{lb} = \mathbb{E}_{\tau\sim\mathcal{D},q_\phi(z_\alpha|\tau)}\left[\sum_{t,i}\log \pi^i_\theta(a^i_t|s_t,z^i_\alpha)\right] - \mathbb{E}_{\tau\sim\mathcal{D}}\left[D_{\mathrm{KL}}(q_\phi(z_\alpha,z_\omega|\tau)||p_\theta(z_\alpha,z_\omega))\right]\ . \tag{10}$$

The first term simply relates to trajectory reconstruction, inducing our agent-wise policies π^i_θ to behave similarly to the observed trajectories in the dataset. The second term is a regularization term

involving our two latent parameters, which we further simplify using assumptions used in previous multi-level VAE models [67]. First, we assume that the posterior distribution is factorizable when conditioned on a particular trajectory, as follows,

$$q_\phi(z_\alpha, z_\omega|\tau) = q_\phi(z_\alpha|\tau)q_\phi(z_\omega|\tau) \tag{11}$$

$$= \left[\prod_i q_\phi(z_\alpha^i|\tau)\right] q_\phi(z_\omega|\tau)\,, \tag{12}$$

and similarly for the prior,

$$p_\theta(z_\alpha, z_\omega) = p_\theta(z_\alpha|z_\omega)p_\theta(z_\omega) \tag{13}$$

$$= \left[\prod_i p_\theta(z_\alpha^i|z_\omega)\right] p_\theta(z_\omega)\,. \tag{14}$$

We next simplify the KL-divergence component of (10) as follows by combining it with (12) and (14):

$$D_{\mathrm{KL}}(q_\phi(z_\alpha, z_\omega|\tau)||p_\theta(z_\alpha, z_\omega)) \tag{15}$$

$$= \int_{z_\alpha, z_\omega} q_\phi(z_\omega, z_\alpha|\tau) \log \frac{q_\phi(z_\alpha, z_\omega|\tau)}{p_\theta(z_\alpha, z_\omega)} d_{z_\alpha} d_{z_\omega} \tag{16}$$

$$= \int_{z_\alpha, z_\omega} q_\phi(z_\alpha|\tau)q_\phi(z_\omega|\tau) \log \frac{q_\phi(z_\alpha|\tau)q_\phi(z_\omega|\tau)}{p_\theta(z_\alpha|z_\omega)p_\theta(z_\omega)} d_{z_\alpha} d_{z_\omega} \tag{17}$$

$$= \int_{z_\alpha, z_\omega} \left[q_\phi(z_\alpha|\tau)q_\phi(z_\omega|\tau) \log \frac{q_\phi(z_\alpha|\tau)}{p_\theta(z_\alpha|z_\omega)} + q_\phi(z_\alpha|\tau)q_\phi(z_\omega|\tau) \log \frac{q_\phi(z_\omega|\tau)}{p_\theta(z_\omega)}\right] d_{z_\alpha} d_{z_\omega} \tag{18}$$

$$= \int_{z_\alpha, z_\omega} q_\phi(z_\omega|\tau) \prod_j q_\phi(z_\alpha^j|\tau) \sum_i \log \frac{q_\phi(z_\alpha^i|\tau)}{p_\theta(z_\alpha^i|z_\omega)} d_{z_\alpha} d_{z_\omega}$$
$$+ \int_{z_\omega} q_\phi(z_\omega|\tau) \log \frac{q_\phi(z_\omega|\tau)}{p_\theta(z_\omega)} d_{z_\omega} \underbrace{\int_{z_\alpha} q_\phi(z_\alpha|\tau) d_{z_\alpha}}_{=1} \tag{19}$$

$$= \sum_i \int_{z_\alpha, z_\omega} q_\phi(z_\omega|\tau) \left(\prod_j q_\phi(z_\alpha^j|\tau)\right) \log \frac{q_\phi(z_\alpha^i|\tau)}{p_\theta(z_\alpha^i|z_\omega)} d_{z_\alpha} d_{z_\omega} + D_{\mathrm{KL}}(q_\phi(z_\omega|\tau)||p_\theta(z_\omega)) \tag{20}$$

$$= \sum_i \int_{z_\alpha^i, z_\omega} q_\phi(z_\omega|\tau)q_\phi(z_\alpha^i|\tau) \log \frac{q_\phi(z_\alpha^i|\tau)}{p_\theta(z_\alpha^i|z_\omega)} d_{z_\alpha^i} d_{z_\omega} \left[\prod_{j\neq i} \underbrace{\int_{z_\alpha^j} q_\phi(z_\alpha^j|\tau) d_{z_\alpha^j}}_{=1}\right]$$
$$+ D_{\mathrm{KL}}(q_\phi(z_\omega|\tau)||p_\theta(z_\omega)) \tag{21}$$

$$= \mathbb{E}_{q_\phi(z_\omega|\tau)} \left[\sum_i D_{\mathrm{KL}}(q_\phi(z_\alpha^i|\tau)||p_\theta(z_\alpha^i|z_\omega))\right] + D_{\mathrm{KL}}(q_\phi(z_\omega|\tau)||p_\theta(z_\omega)) \tag{22}$$

Combining this result with (10) and additionally modulating the KL-terms in the lower bound as in β-VAEs [72], our overall objective simplifies to

$$J_{lb} = \mathbb{E}_{\tau\sim\mathcal{D}, z_\alpha\sim q_\phi(z_\alpha|\tau)} \left[\sum_{t,i} \log \pi_\theta^i(a_t^i|s_t, z_\alpha^i)\right] \tag{23}$$

$$-\beta \Bigg[\mathbb{E}_{\tau\sim\mathcal{D}, z_\omega\sim q_\phi(z_\omega|\tau)} \Big[\sum_i D_{\mathrm{KL}}(q_\phi(z_\alpha^i|\tau)||p_\theta(z_\alpha^i|z_\omega))\Big] \tag{24}$$

$$+\mathbb{E}_{\tau\sim\mathcal{D}} \left[D_{\mathrm{KL}}(q_\phi(z_\omega|\tau)||p_\theta(z_\omega))\right]\Bigg]\,. \tag{25}$$

A.2 Experiment Details and Hyperparameters

This section provides an overview of the details for our experiments.

A.2.1 Data Generation Details

The multiagent trajectory data analyzed in this paper is generated using the Acme RL library [75], using the TD3 algorithm [76] in a decentralized fashion, with dataset management handled using RLDS [77]. Each agent uses a 2-layer MLP (256 hidden units for each layer) for its TD3 network (using the vanilla TD3 network specifications in Acme), with the hyperparameters used for data generation summarized for each domain in Table 4. Note that the large number of training trials/seeds used in this data generation pipeline serve to produce a wide variety of agent behaviors in the dataset subsequently analyzed by MOHBA.

Table 4: Hyperparameters used for data generation. Values in braces indicate hyperparameter sweeps.

Parameter	Hill-climbing	Coordination Game	HalfCheetah	AntWalker
MARL algorithms used	TD3	TD3	TD3	{TD3, SAC}
# agents	3	2	2	4
Episode steps	50	50	200	300
# steps per training trial	1e5	2e5	2e5	2e5
TD3 / SAC batch size	256	256	256	{32, 256}
TD3 / SAC learning rates	5e-5	5e-5	5e-4	{1e-3 to 9e-3}
TD3 σ	0.1	0.1	0.1	0.1
TD3 target σ	0.1	0.1	0.1	0.1
TD3 τ	0.005	0.005	0.005	0.005
TD3 delay	2	2	2	2
# seeds	50	50	30	50

A.2.2 MOHBA Hyperparameters

We conduct a wide hyperparameter sweep for training MOHBA itself, summarized in Table 5. Our joint and local encoder models each consist of a bidirectional LSTM, followed by a 2-layer MLP head for mapping to latent distribution parameters; a GMM head is used for the joint encoder, and a Gaussian for the local encoder. Our local prior model consists of a 2-layer MLP with Gaussian head, with our joint prior model simply being the learned parameters of a GMM. All models use ReLU for intermediate layer activations. Note that we found that cyclically-annealing [82] the β term in our variational lower bound from 0 to the values specified in Table 5 to help avoid KL-vanishing. All MOHBA and baseline training is conducted using the Adam optimizer [80], with Adam parameters $\beta_1 = 0.9$, $\beta_2 = 0.999$, gradient clipping using a max global norm threshold of 10.0, and learning rates swept over as indicated in the tables.

Table 5: Hyperparameter sweeps for training MOHBA. Values swept over are indicated via braces.

Parameter	Value
Training steps	1e5
Batch size (# trajectories)	128
Latent z_ω and z_α^i dimensionality	{4, 8}
Hidden units (joint encoder/local prior/local encoder MLPs)	{64, 128}
Hidden units (joint encoder /local encoder LSTMs)	{64, 128}
Hidden units (reconstructed policy MLP)	32
GMM mixture size (joint prior/joint encoder)	8
Adam optimizer learning rates	{1e-3, 1e-4}
KL-loss β weighing term	{1e-4, 1e-2}
KL-loss cyclical annealing period	{5e3, 1e4}
# seeds	3

A.2.3 Baseline Model Hyperparameters

We similarly conduct a wide sweep over hyperparameters for the considered baselines, summarized in Table 6.

Table 6: Hyperparameter sweeps for baselines. Values swept over are indicated via braces.

Parameter	LSTM Baseline	VAE Baseline
Training steps	1e5	1e5
Batch size (# trajectories)	128	128
Latent z_ω dimensionality	N/A	{4, 8}
Hidden units (joint encoder/local prior/local encoder MLPs)	N/A	{64, 128}
Hidden units (joint encoder /local encoder LSTMs)	{64, 128}	{64, 128}
Hidden units (reconstructed policy MLP)	32	32
GMM mixture size (joint prior/joint encoder)	N/A	8
Adam optimizer learning rates	{1e-3, 1e-4}	{1e-3, 1e-4}
KL-loss β	N/A	{1e-4, 1e-2}
KL-loss cyclical annealing period	N/A	{5e3, 1e4}
# seeds	3	3

A.2.4 Computational Details

For MARL trajectory data generation, we used an internal CPU cluster for both the 3-agent hill-climbing and 2-agent coordination domains, using TPUs for only the multiagent MuJoCo data generation. For training MOHBA itself, we used TPUs for the 3-agent hill-climbing and 2-agent coordination domains, and a Tesla V100 GPU cluster for the MuJoCo environment. For training the LSTM and VAE baselines, we used Tesla P100 GPU clusters.

A.2.5 Concept Discovery Framework

This section describes details of how we apply the completeness-aware concept-based explanation framework of Yeh et al. [13] to discover interesting concepts in our setting.

Given a characteristic of interest (e.g., the level of dispersion of agents), we define a training set consisting of joint latents z_ω and class labels y (e.g., classes corresponding to different intervals of team returns). Yeh et al. [13] seek to identify a set of concept vectors that are sufficient for predicting the labels given the inputs. Specifically, they let $C = \{c_j\}_{j=1}^m$ denote the set of concepts, which are unique vectors where $c_j \in \mathbb{R}^{D_\omega}\ \forall j$. Normalizing z_ω, we can then use the inner product $\langle z_\omega, c_j \rangle$ as a similarity measure between z_ω and concept c_j. The *concept product* is defined $\nu_{\boldsymbol{c}}(z_\omega) = \text{TH}(\langle z_\omega, c_j \rangle, \kappa) \in \mathbb{R}^m$, where $\text{TH}(\cdot, \kappa)$ clips values less than κ to 0. Normalizing the concept product yields the *concept score* $\hat{\nu}_{\boldsymbol{c}}(z_\omega) = {}^{\nu_{\boldsymbol{c}}(z_\omega)}/_{||\nu_{\boldsymbol{c}}(z_\omega)||_2} \in \mathbb{R}^m$, where elements provide a measure of similarity of the input z_ω to each of the m concept vectors.

Using these definitions, we can gauge the representational power of z_ω by learning a mapping $g : \hat{\nu}_{\boldsymbol{c}}(z_\omega) \rightarrow y$. In practice, g is a simple model (e.g., shallow network or linear projection) so as to gauge the expressivity of the latent space. Given a mapping g, we use the classification accuracy as a 'completeness score' [13] for the set of concepts C, defined $\eta = \sup_g P_{z_\omega, y \sim V}\left[y = \arg\max_{y'} g(\nu_{\boldsymbol{c}}(z_\omega))\right]$, where V is a validation set. Importantly, this approach permits us to compute class-conditioned Shapley values, called ConceptSHAP in the framework of [13]. Specifically, for a given class k, the class-conditioned ConceptSHAP value for each concept c_j is defined,

$$\lambda_j(\eta_k) = \sum_{S \subseteq C \setminus c_j} = \frac{(m - |S| - 1)!|S|!}{m!}\left[\eta_k(S \cup \{c_j\}) - \eta_k(S)\right] , \tag{26}$$

where η_k is the completeness score for class k (computed simply as the classification accuracy of the model for the subset of validation points with ground truth label k). ConceptSHAP provides a measure of importance of each concept c_j for predicting the outcomes associated with a given class, which we can then use to identify the trajectories. The experiments in our main paper use the above

setup to both quantitatively evaluate z_ω in terms of representation power, and also reveal interesting concepts associated with relevant characteristics in the domain.

For each of the prediction problems considered in the main paper (agent dispersion and agent returns), we create an 80-20 training-validation data split (over 5 classes). For concept generation we use K-means with 16 and 24 clusters, a 2-layer MLP (with 8 hidden units per layer) for the prediction head g, training with a batch size of 64, and a concept threshold κ of 0.0 and 0.3 for the dispersion and agent return experiments, respectively, and train the prediction head for $1e4$ steps. As in Yeh et al. [13], we use KernelSHAP [83] to approximate ConceptSHAP efficiently.

A.3 Additional Results

A.3.1 Additional Large-scale Experiments

MultiAgent MuJoCo AntWalker Domain Results. We also consider the MultiAgent MuJoCo AntWalker domain, wherein 4 agents each control one of 4 ant legs to coordinate movement towards the $+x$ direction (Fig. 6a). To collect data for this domain, we conduct a wider MARL parameter sweep using both the TD3 and SAC algorithms, with varying training batch sizes and learning rates to gather a widely-varying dataset of behaviors. We subsequently train MOHBA on this data, visualizing the learned behavior clusters in Fig. 6b. We observe several behavior clusters of interest; notably, a large joint cluster exists in the top-right region of the joint and local returns, which, upon inspection of underlying trajectory videos, corresponds to cases where agents attain extremely low return. Similarly, there exists a smaller cluster in the lower-left region of the joint returns that also attains extremely low performance. The remaining clusters correspond to the agents displaying various ant-poses, and moving only incrementally. One exceptional cluster also exists in the left region of the joint behavior space, which attains medium-level return (points that are primarily red in color). On closer inspection, the AntWalker behavior in this cluster corresponds to one of the agents learning a reasonably good walking gait, while the remaining three agents remain stationary.

Application to externally-trained policies: team-based hide-and-seek game. We next consider the application of MOHBA to pre-existing policies trained by external teams. Specifically, we consider the aforementioned OpenAI hide-and-seek environment, wherein two teams of two agents (hiders and seekers) compete against one another in a rich, high-dimensional environment with various dynamic objects (boxes and ramps) that the agents can interact with. OpenAI has open-sourced policy checkpoints manually annotated by human experts as exhibiting various distinctive multiagent behaviors at key stages of training in `github.com/openai/multi-agent-emergence-environments`. We consider four distinctive policy checkpoints that each correspond to the following human-annotated labels: A) 'running and chasing', B) 'fort building', C) 'ramp use', and D) 'ramp defense'.

The state-space for each of the agents at each timestep of the trajectory is 100-dimensional, consisting of its own state (position, rotation, and velocity information), states of the other 3 agents, and the states of 3 boxes and one ramp in the environment (position, velocity, and box size information); each agent's action space consists of a 3-dimensional force vector, and a 'glue' and 'lock' action for interacting with other objects. Overall, this yields a state-action space with dimensionality (4 agents $\times 105$ state-actions), significantly larger than the (2 agents $\times 9$ state-actions) of the HalfCheetah environment above. We collect 100 trajectories per policy checkpoint, with each trajectory being 200 decision-steps long. Note that these trajectories have a wide distribution of behaviors, as agent and object initializations are also random in each episode.

We then mix the trajectories collected from all of the above policy checkpoints together, then train MOHBA on this shuffled dataset. As usual, note that we provide no reward or return information to MOHBA. Figure 7 visualizes the behavior spaces discovered by MOHBA in the hide-and-seek domain. Agents 0 and 1 in this figure correspond to 'hiders', whereas agents 2 and 3 are 'seekers'. We label each of the trajectories in this figure with the human-annotated behavior labels provided by OpenAI.

In Fig. 7, we observe the presence of clear behavior clusters that correspond well to the expert policy checkpoint labels, both at the joint and local agent levels. Interestingly, for the seekers (agents 2 and 3), policy A ('running and chasing') is highly distinctive and well-separated from the other behaviors. Interestingly, despite the order of emergent behaviors in the original hide-and-seek MARL training being A $\rightarrow$ B $\rightarrow$ C $\rightarrow$ D, policies B ('fort building') and D ('ramp defense') appear to be behaviorally

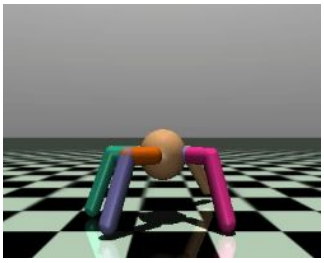

(a)

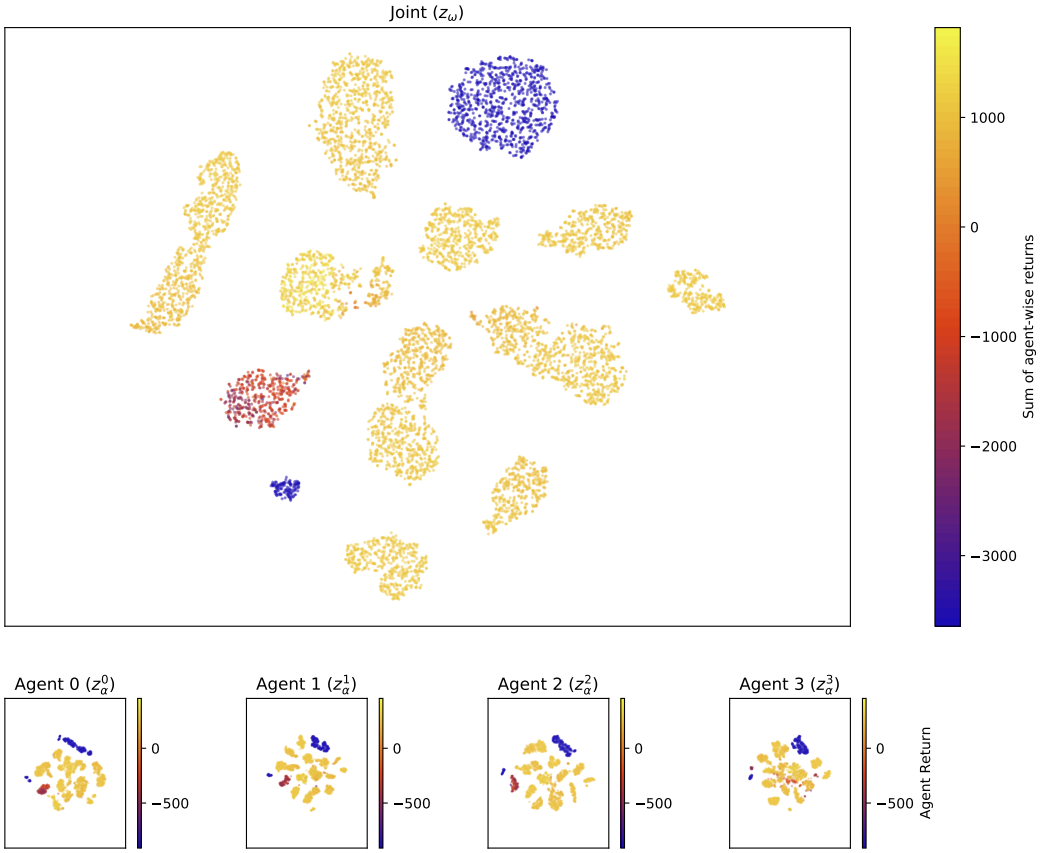

(b)

Figure 6: Results for Multiagent MuJoCo AntWalker domain. (see interactive version here). (a) This domain involves 4 agents, each controlling one of the ant legs to coordinate movement towards the $+x$ direction. (b) Behavior space learned by MOHBA in the AntWalker domain.

slightly closer to one another than C ('ramp use') and D, namely in the joint space and also in that of the seeker (agent 2 and 3) latent spaces. One hypothesis is that this could perhaps be due to both the 'fort building' and 'ramp defense' policies being associated with situations where the seekers cannot easily find the hiders, due to the hiders using obstacles to block entrances (B) and moving ramps to prevent their effective use (D). Overall, these experiments help to validate MOHBA's learned latent spaces using policy labels manually annotated by human experts, and also highlight the applicability of our algorithm in domains with large state spaces.

A.3.2 Additional Baseline Results

Figures 8 and 9 provide additional results for the baseline comparisons conducted in the main paper. Specifically, (a) in each figure provides an expanded comparison of ICTD (with a sweep over the #

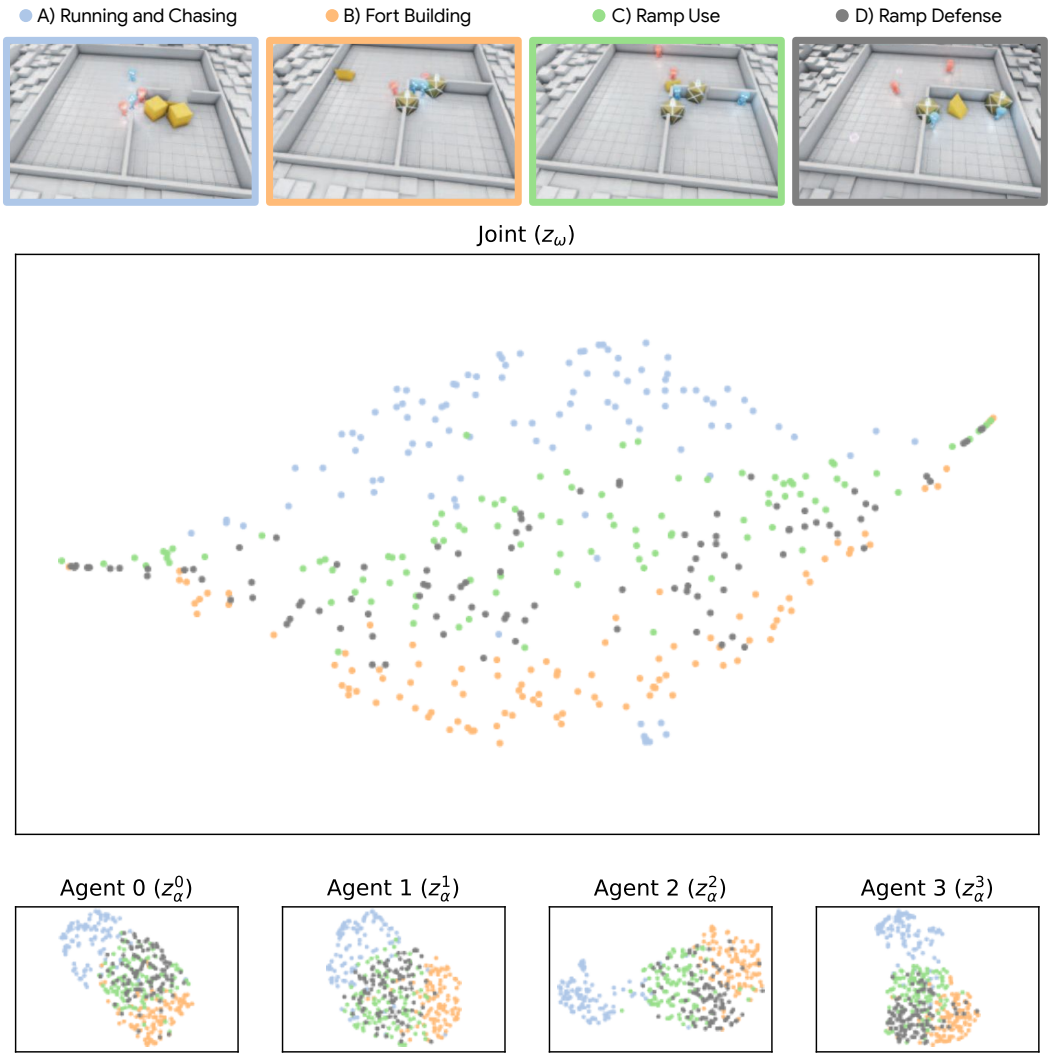

Figure 7: Results for the OpenAI hide-and-seek environment [10], wherein two teams of two agents (hiders and seekers) compete against one another in a rich, high-dimensional environment with various dynamic objects (boxes and ramps) that the agents can interact with. We mix the trajectories collected from all of the above policy checkpoints together, then train MOHBA on this shuffled dataset. Using MOHBA, we observe the presence of clear behavior clusters that correspond well to the expert policy checkpoint labels, both at the joint and local agent levels, despite our algorithm not having access to the explicit policy labels during training. Domain screenshots reproduced with permission from Baker et al. [10].

of clusters in K-means). In (b) of each figure, we visualize the convergence of the APL throughout training for MOHBA and the baselines. Subfigures (c) and (d), respectively, show a PCA and UMAP projection of the latent space discovered by the LSTM baseline (recall from the main paper that 'joint embeddings' used for the LSTM are simply the final hidden state). Likewise, subfigures (e) and (f) show the same projections for the VAE baseline.

As especially evident in the coordination domain (Fig. 9), the joint LSTM baseline embeddings (whether using PCA or UMAP projections, Figs. 9c and 9d, respectively) do not reveal to the fairly interpretable 3 clusters of coordinated behaviors discussed in the main paper. By contrast, the VAE baseline (in both the PCA and UMAP case, Figs. 9e and 9f, respectively) does produce these clusters; despite this, note that the key limitation of this baseline is its non-hierarchical nature, which makes

identification of the local-to-joint behavioral correspondences noted in the main paper significantly more difficult.

	APL	ICTD		
		K=4	K=8	K=16
LSTM	4.8 ± 0.1	0.60 ± 0.15	0.51 ± 0.17	0.47 ± 0.19
VAE	6.9 ± 0.4	0.44 ± 0.11	0.30 ± 0.14	0.18 ± 0.13
MOHBA	1.3 ± 0.1	0.46 ± 0.13	0.31 ± 0.13	0.17 ± 0.13

(a) Action-prediction loss (APL) and intra-cluster trajectory distance (ICTD).

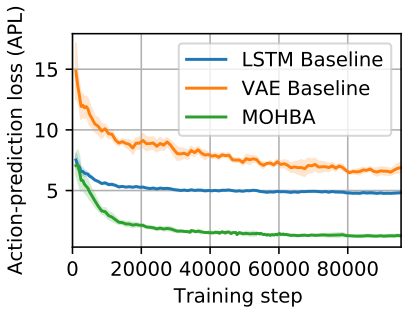

(b) APL convergence throughout training.

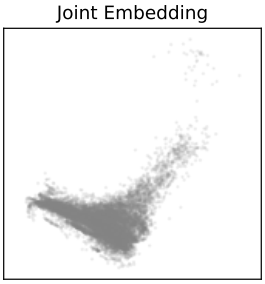

(c) LSTM Baseline (PCA projection)

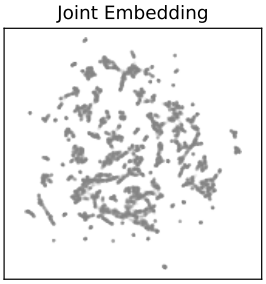

(d) LSTM Baseline (UMAP projection)

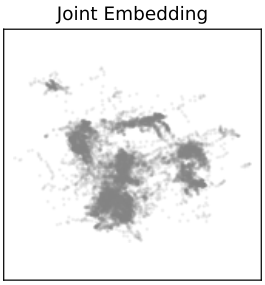

(e) VAE Baseline (PCA projection)

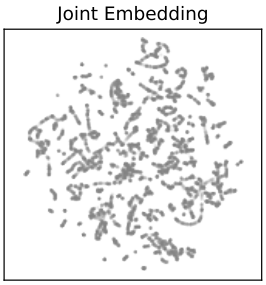

(f) VAE Baseline (UMAP projection)

Figure 8: Baseline comparisons (hill-climbing domain).

A.4 Hyperparameter Ablations and Effects on Latent Spaces

This section conducts an analysis of the effect of key hyperparameters on the latent spaces learned by MOHBA. We focus our analysis on the KL-loss β term in the training objective, alongside the latent z_ω and z_α dimensionality. We both compare the policy reconstruction loss (5) across ablations to attain a quantitative comparison of the quality of the latent encodings, and additionally compare the structure of the learned latent spaces themselves as a function of these parameters for a qualitative understanding.

	APL	ICTD		
		K=4	K=8	K=16
LSTM	2.9 ± 0.1	0.41 ± 0.15	0.40 ± 0.14	0.34 ± 0.15
VAE	5.0 ± 0.3	0.18 ± 0.11	0.17 ± 0.11	0.16 ± 0.10
MOHBA	2.4 ± 0.3	0.18 ± 0.12	0.17 ± 0.10	0.16 ± 0.10

(a) Action-prediction loss (APL) and intra-cluster trajectory distance (ICTD).

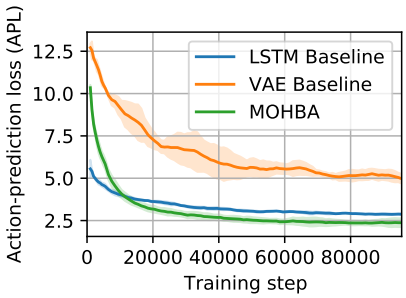

(b) APL convergence throughout training.

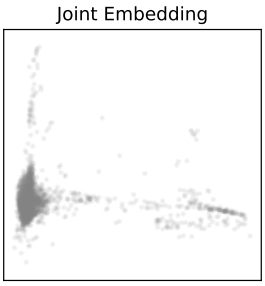

(c) LSTM Baseline (PCA projection)

(d) LSTM Baseline (UMAP projection)

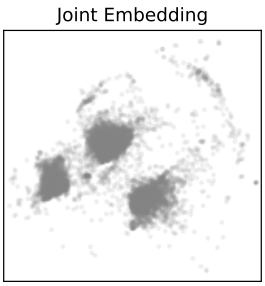

(e) VAE Baseline (PCA projection)

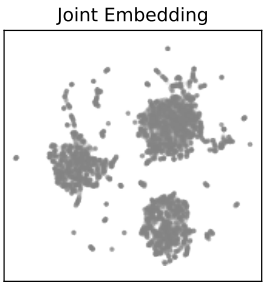

(f) VAE Baseline (UMAP projection)

Figure 9: Baseline comparisons (coordination game).

First, in terms of the raw policy reconstruction loss, we find in Figs. 10a, 11a and 12a that the latent dimensionality has a higher impact on policy reconstruction performance than the weighing term β; intuitively, increasing latent dimensionality leads to better reconstruction (lower loss) due to the latent space being able to encode more behavioral information about the agent trajectories. By contrast, the effects of the KL weighing term are more negligible in terms of reconstruction loss.

Second, we inspect the effects of these hyperparameter sweeps on the learned latent distributions themselves. Specifically, the respective panels (b)-(e) of each of Fig. 10, Fig. 11, and Fig. 12 visualize the change in latent space structure as a function of the latent dimensionality and β. At a high-level, prominent behavioral clusters mentioned in the main text are re-discovered throughout these parameter sweeps (e.g., the three local clusters for the hill climbing environment, the joint and local clusters for the coordination environment, and the various walking gait clusters for the HalfCheetah environment). For the more complex latent spaces (e.g., HalfCheetah), increasing the

dimensionality of z tends to increase the number of joint clusters identified (e.g., compare Fig. 12c versus Fig. 12e); this is intuitive as a larger latent space results in a richer encoding, capable of distinguishing more nuanced behaviors. Increasing the KL β term from $1e-4$ to $1e-2$ tends to result in clusters that overlap more / are 'softer' and slightly less distinguishable (e.g., comparing z_ω in Fig. 12c versus Fig. 12d); this also aligns well with intuition, as increasing the β term prioritizes the KL divergence between the posterior and prior, which deprioritizes disentangling the behaviors for the policy reconstruction term (5).

Overall, these results provide us intuition in terms of the role of these hyperparameters in the behavior clusters learned. At a high level, it appears that the sensitivity of the results to these hyperparameters is fairly low (in the range of values explored in these experiments), thus allowing the high level behaviors discovered to remain reasonably distinctive across the various sweeps.

A.5 Additional Dataset Details / Reward Distributions

This section provides additional details and statistics regarding the trajectory datasets used for evaluation. Specifically, one of the core properties of datasets typically used for offline RL is the inclusion of a large number of sub-optimal and random trajectories [84]. As noted earlier, the trajectory data for the agents in our experiments is collected from numerous underlying MARL training runs for each domain. To help ensure the collection and analysis of a diverse set of behaviors including sub-optimal ones, we not only collect trajectories at the end of MARL training, but rather from policy checkpoints throughout all of training. All such trajectories, including those stemming from randomly-initialized agent policies at the beginning of training, are shuffled together and used to simultaneously train MOHBA.

Table 7: Trajectory return statistics for each of the datasets analyzed.

Domain	% of trajectories with total return $< 0.5\times$ (maximum observed return)
HalfCheetah (2 agents)	92.69%
AntWalker (4 agents)	22.47%
Hill-climbing	23.91%
Coordination game	11.83 %

Here we more closely inspect our datasets to better understand the distribution of agent behaviors. At a high level, we first note that our datasets consist of a significant proportion of sub-optimal trajectories. Specifically, in Table 7, we note the percent of trajectories in each of the considered datasets that attain less than 50% of maximum observed return. Note that in the high-dimensional MultiAgent MuJoCo environments especially, a large proportion of low-reward trajectories exist in the dataset, with the HalfCheetah dataset being a particularly notable one where 92.69% of datasets attain less than 50% of max observed return.

We additionally provide a more detailed overview of trajectory returns in each of Figs. 13a, 14a, 15a and 16a. These figures visualize the distribution of individual agent returns in each of the considered environments (respectively, hill-climbing, coordination game, 2-agent HalfCheetah, and 4-agent AntWalker). Notably, many of the trajectories in the HalfCheetah domain are skewed towards medium and low-return behaviors, with very few high-return trajectories present (Fig. 13a). Interestingly, in the AntWalker dataset we observe a bimodal return distribution (seemingly consisting of very low return and very high return trajectories, as seen in Fig. 14a). Closer inspection of this domain reveals that a large number of training runs result in highly sub-optimal behaviors with very low returns; in Fig. 14b, we visualize the distribution of returns with these low-return trajectories excluded, observing a similar distribution to the HalfCheetah dataset (consisting primarily of medium-return trajectories). Similarly, a large proportion of trajectories with extremely low returns exist in the hill-climbing and coordination game domains (Figs. 15a and 16a); we verified that these low-return trajectories consist primarily of random agent behaviors collected early in training. Overall, this analysis is helpful in determining that the analyzed datasets exhibit a wide range of trajectories (in terms of agent returns), covering random behaviors, sub-optimal behaviors, and high-return behaviors, similar to typical offline RL datasets [84].

As part of this investigation, we also analyze the discovered behavior spaces (both at joint and local agent levels) with respect to the return distributions. Specifically, Figs. 13b, 14c, 15b and 16b visualize

the behavior spaces learned by MOHBA, which are then labeled by the ground truth return corresponding to each trajectory. Interestingly, despite MOHBA not using *any* reward or return information in learning agent behavior spaces, clear clusters corresponding to low-return (random/early-training trajectories), medium-return trajectories, and high-return trajectories are automatically discovered in all of the considered domains. For example, in the hill-climbing environment, many of the trajectories corresponding to low returns are clustered in the center of the joint latent space in Fig. 15b; in the HalfCheetah environment, a prominent cluster of high-return trajectories is visible in the top-left and bottom-left local latent spaces of agents 0 and 1, respectively (Fig. 14c); in the AntWalker environment, the lowest-return trajectories are clustered in distinctive regions both at the joint and local level, with a medium-return trajectory set also visible in the latent spaces (Fig. 14c). Overall, these results indicate the richness of the learned latent spaces in terms of not only raw trajectories but also their capacity to cluster trajectories that exhibit similar performance, even without observing the reward function.

A.6 Visualizing z_ω and z_α

This section summarizes the procedure used to generate the behavior space figures associated with z_ω and z_α. The visualization procedure we use is as follows:

1. We train MOHBA using the offline behavior datasets of interest.
2. Following training of MOHBA, we pass each trajectory τ through both the joint encoder $q_\phi(z_\omega|\tau)$ and the agent-wise local encoders $q_\phi(z_\alpha^i|\tau)$, sampling a joint latent z_ω and a set of local latents z_α^i for all N agents accordingly. Thus, for K such trajectories we obtain a set of latent parameters $\{(z_\omega, z_\alpha^1, \cdots, z_\alpha^N)_k\}_{k=1}^K$.
3. As the latent parameters are high-dimensional in nature, we visualize their 2D projection (e.g., using Principal Component Analysis), thus yielding the behavior space visualizations such as those in Fig. 3a.

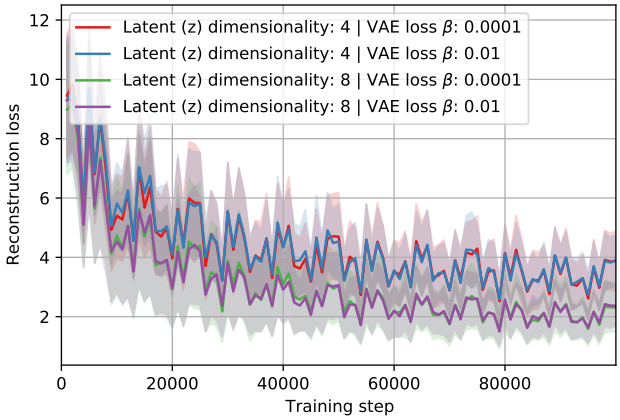

(a)

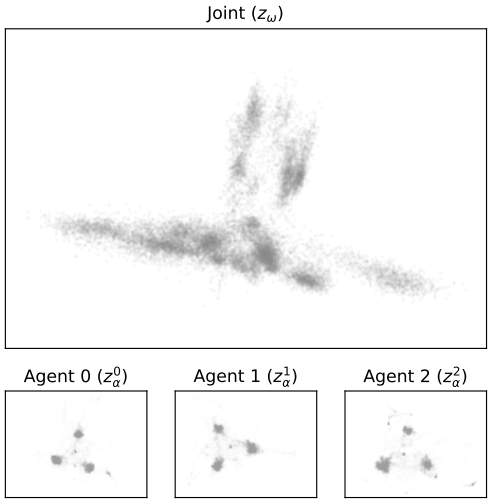

(b) Latent z dimensionality: 4, VAE KL-loss β: 1e-4

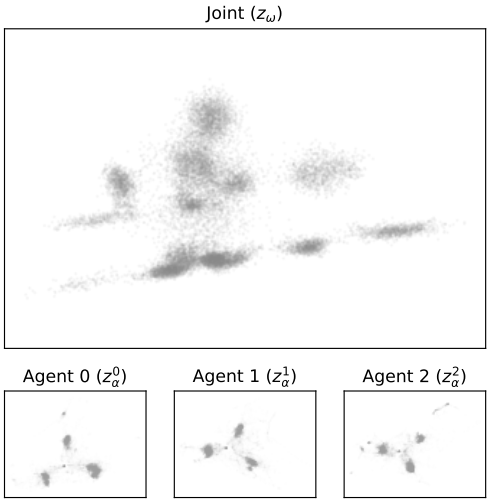

(c) Latent z dimensionality: 4, VAE KL-loss β: 1e-2

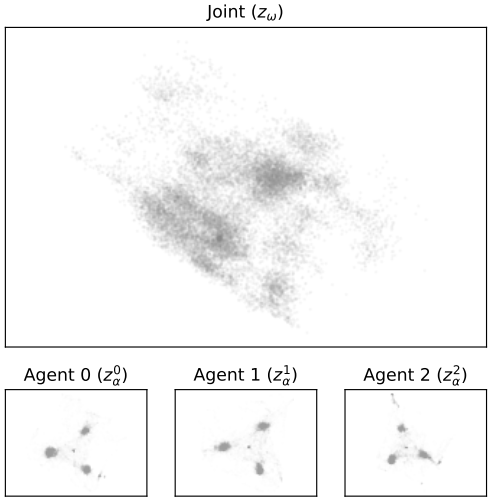

(d) Latent z dimensionality: 8, VAE KL-loss β: 1e-4

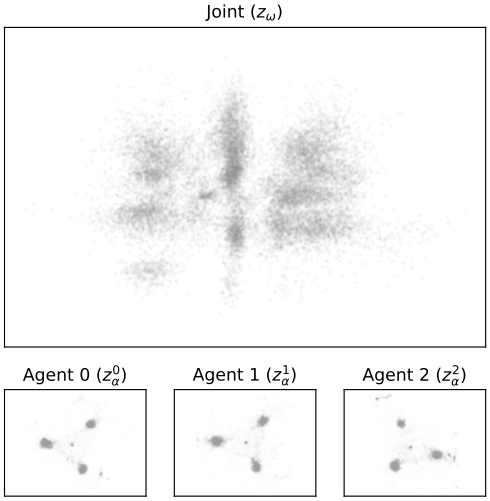

(e) Latent z dimensionality: 8, VAE KL-loss β: 1e-2

Figure 10: Ablations over hyperparameters for 3-agent hill climbing environment. (a) visualizes the reconstruction policy loss throughout MOHBA training. (b)-(e) visualize the change in latent space for each of the final MOHBA models learned over these ablations.

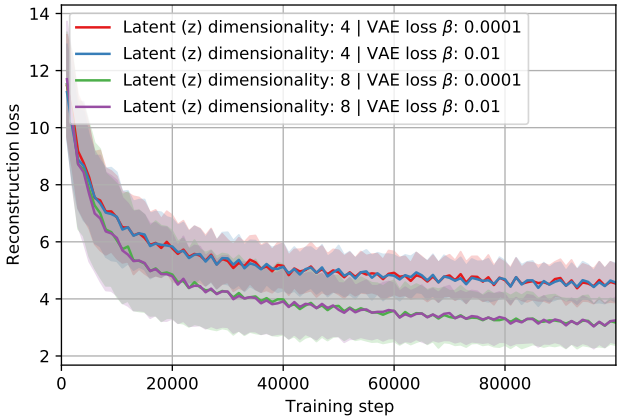

(a)

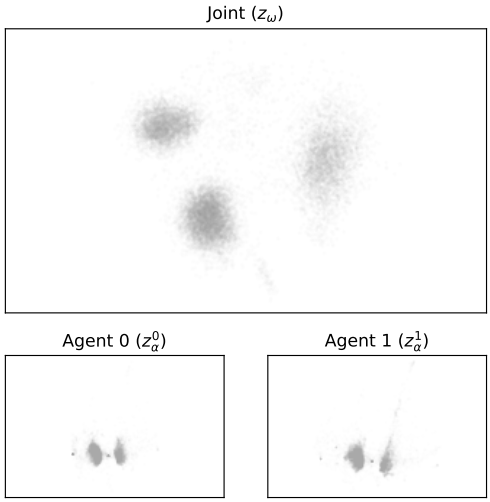

(b) Latent z dimensionality: 4, VAE KL-loss β: 1e-4

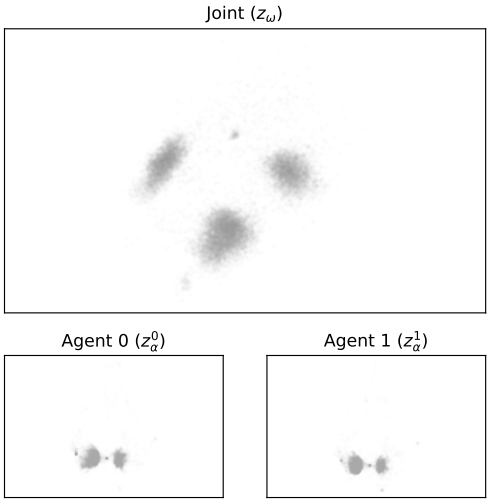

(c) Latent z dimensionality: 4, VAE KL-loss β: 1e-2

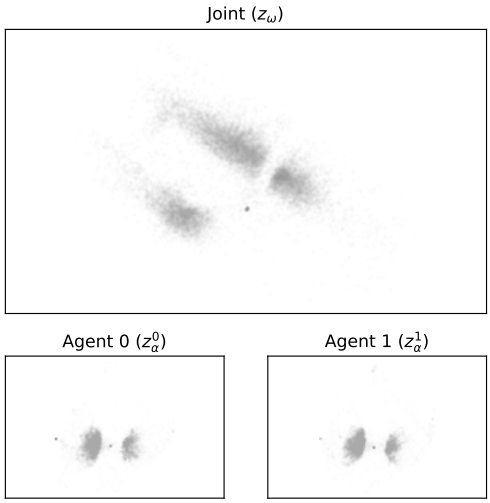

(d) Latent z dimensionality: 8, VAE KL-loss β: 1e-4

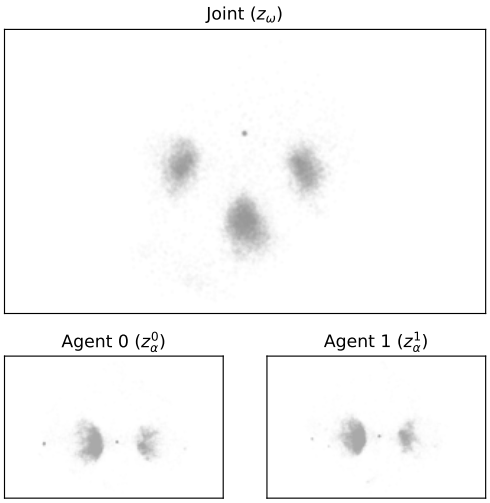

(e) Latent z dimensionality: 8, VAE KL-loss β: 1e-2

Figure 11: Ablations over hyperparameters for 2-agent coordination game. (a) visualizes the reconstruction policy loss throughout MOHBA training. (b)-(e) visualize the change in latent space for each of the final MOHBA models learned over these ablations.

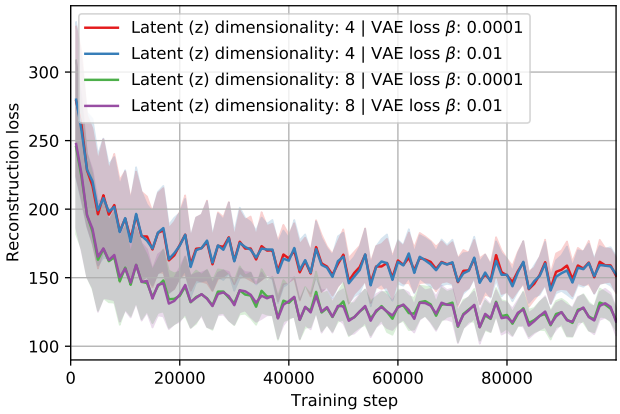

(a)

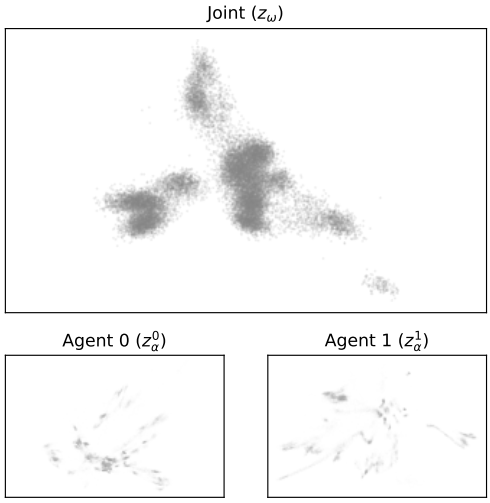

(b) Latent z dimensionality: 4, VAE KL-loss β: 1e-4

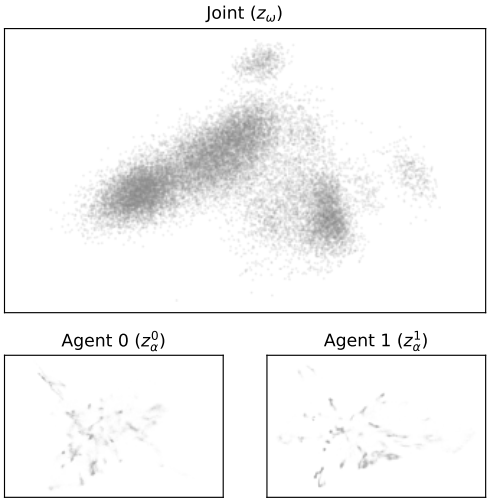

(c) Latent z dimensionality: 4, VAE KL-loss β: 1e-2

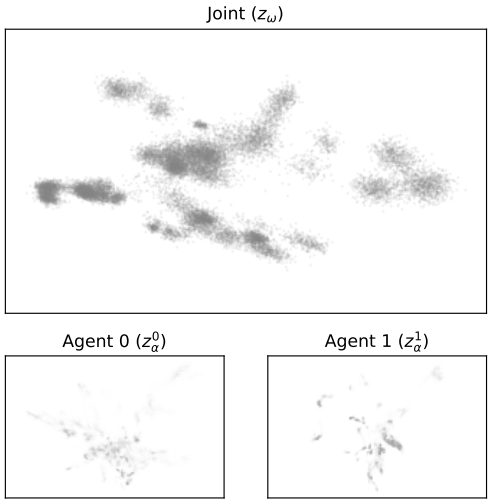

(d) Latent z dimensionality: 8, VAE KL-loss β: 1e-4

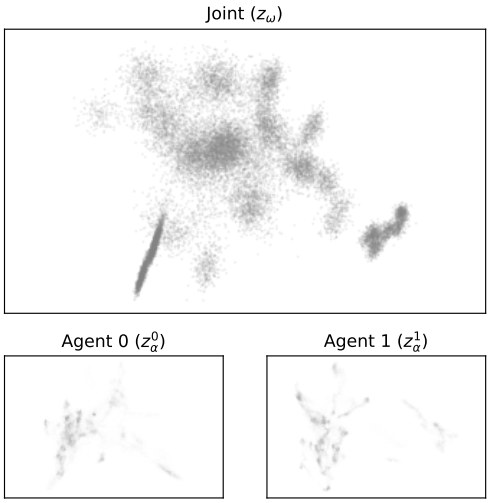

(e) Latent z dimensionality: 8, VAE KL-loss β: 1e-2

Figure 12: Ablations over hyperparameters for Multiagent MuJoCo HalfCheetah. (a) visualizes the reconstruction policy loss throughout MOHBA training. (b)-(e) visualize the change in latent space for each of the final MOHBA models learned over these ablations. Increasing the dimensionality of z tends to increase the number of joint clusters identified (e.g., (c) versus (e)). Increasing the KL β term from $1e-4$ to $1e-2$ tends to result in clusters that overlap more / are 'softer' and slightly less distinguishable (e.g., comparing z_ω in (c) versus (d)).

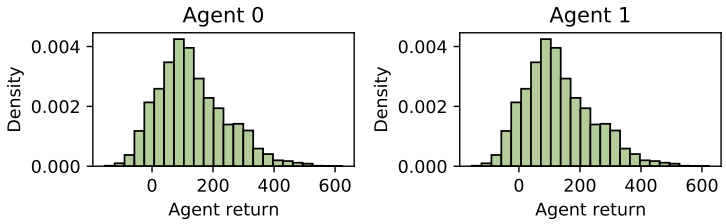

(a) Agent-wise return distribution.

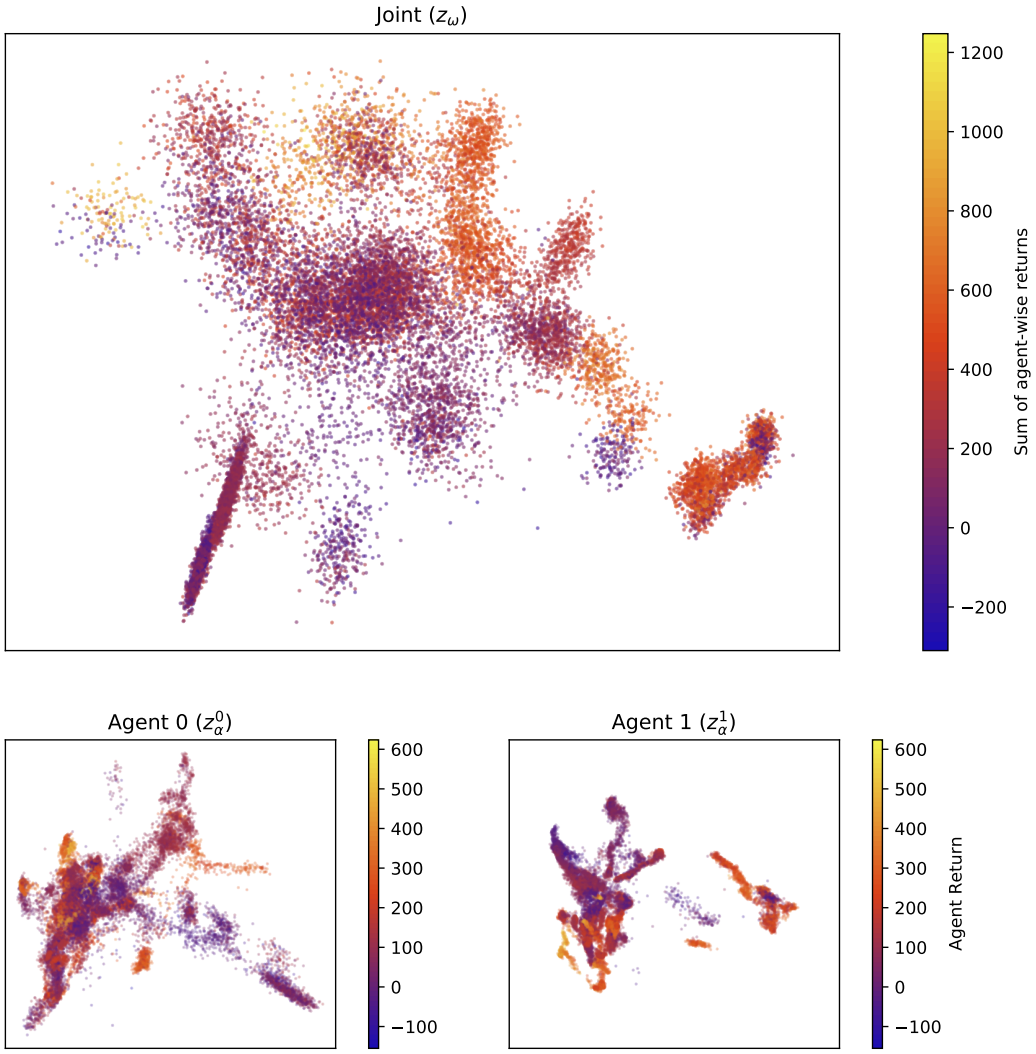

(b) Latent spaces, labeled by trajectory return.

Figure 13: Reward statistics for the Multiagent MuJoCo 2-agent HalfCheetah environment. (a) visualizes the distribution of agent returns in the dataset. (b) visualizes the agent behavior spaces, with trajectories labeled by the return attained.

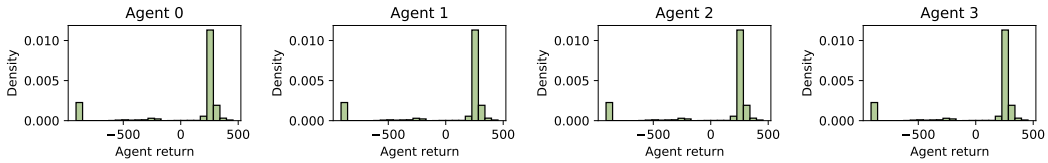

(a) Agent-wise return distribution.

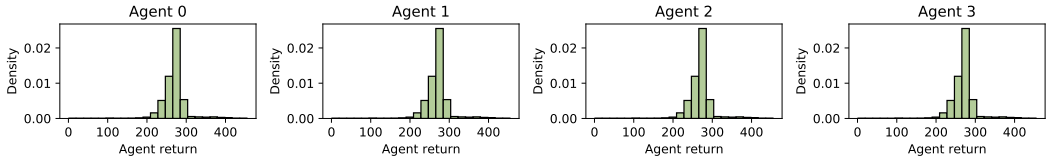

(b) Agent-wise return distribution (anomalous trajectories with returns less than 0 removed).

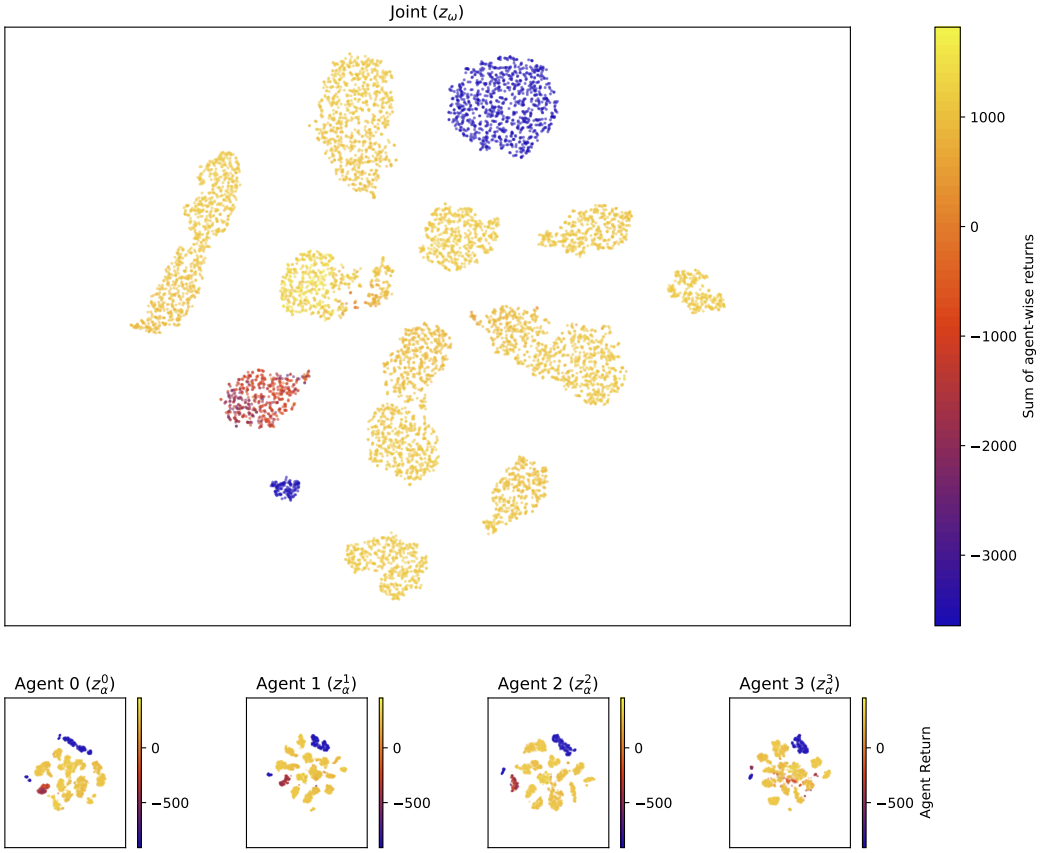

(c) Latent spaces, labeled by trajectory return.

Figure 14: Reward statistics for the Multiagent MuJoCo 4-agent AntWalker environment. (a) visualizes the distribution of agent returns in the dataset. Interestingly, we observe a bimodal return distribution (seemingly consisting of low return and higher return trajectories. Closer inspection reveals that a large number of MARL training runs in this domain result in highly sub-optimal behaviors with very low returns; in (b), we visualize the distribution of returns with these low-return trajectories excluded, which better illustrates the distribution of medium-high reward trajectories in this dataset. (c) visualizes the agent behavior spaces, with trajectories labeled by the return attained.

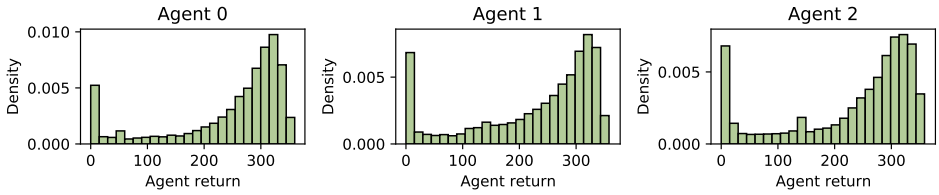

(a) Agent-wise return distribution.

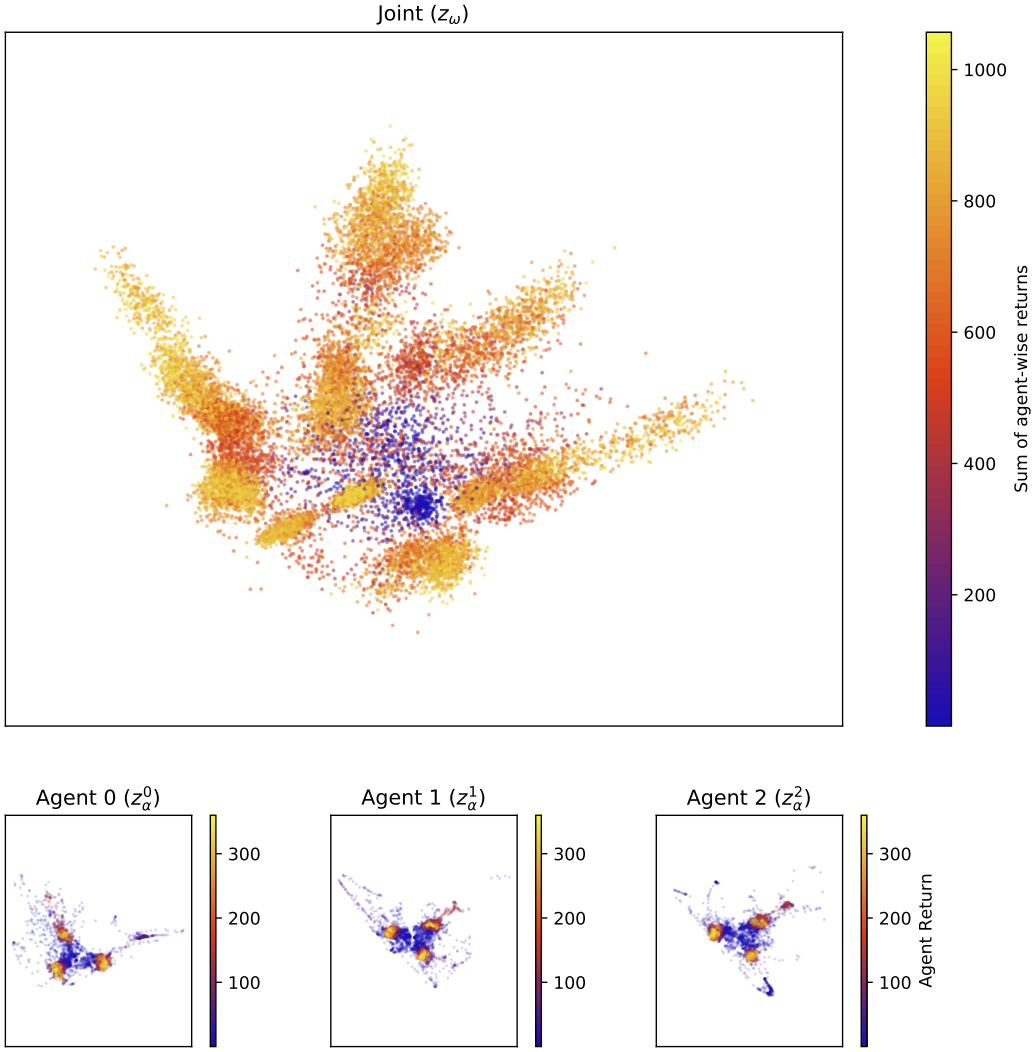

(b) Latent spaces, labeled by trajectory return.

Figure 15: Reward statistics for the 3-agent hill climbing environment. (a) visualizes the distribution of agent returns in the dataset. (b) visualizes the agent behavior spaces, with trajectories labeled by the return attained.

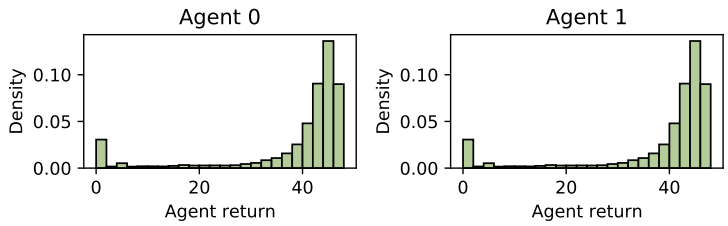

(a) Agent-wise return distribution.

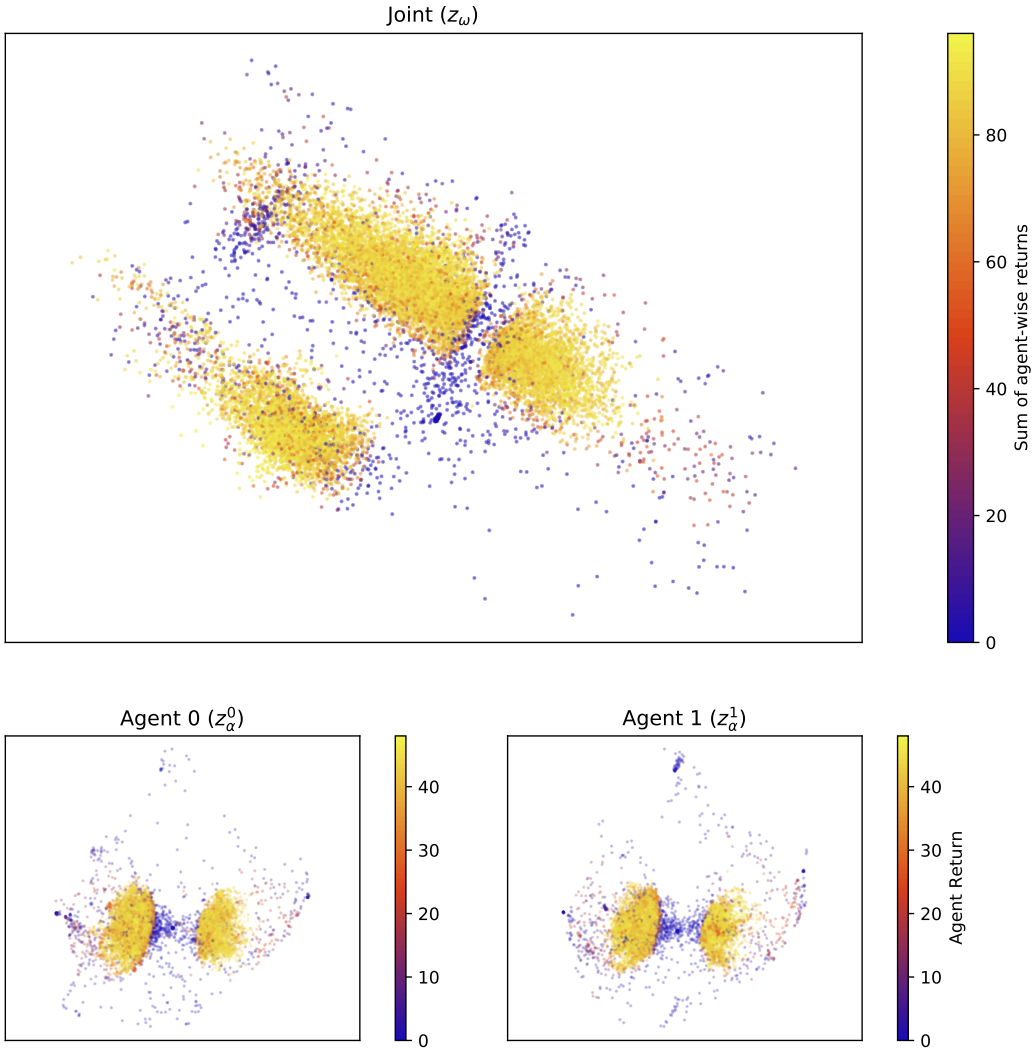

(b) Latent spaces, labeled by trajectory return.

Figure 16: Reward statistics for the 2-agent coordination environment. (a) visualizes the distribution of agent returns in the dataset. (b) visualizes the agent behavior spaces, with trajectories labeled by the return attained.